# Space Time Processing, Environmental-Acoustic Effects

William M. Carey
NUSC, New London, CT 06320

William B. Moseley
NORDA, NSTL, MS 39529

# Naval Underwater Systems Center
Newport, Rhode Island / New London, Connecticut

## PREFACE

This document is an expanded version of an invited paper presented at the 12th International Congress on Acoustics held in Halifax, Nova Scotia, in July, 1986. The sponsors of this work are numerous and the work itself spanned the activities of several institutions, most notably the Naval Research Laboratory and the Naval Oceanographic Research and Development Activity. The results presented in this document were necessarily drawn from the NRL research group which was under the supervision of Dr. Moseley and numerous contractors under the supervision of Dr. Carey. This report, prepared by W. Carey, is issued to document and to make available the results of several years of research.
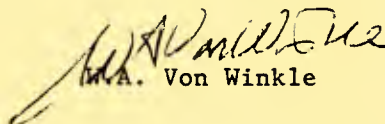

Reviewed and Approved


W. A. Von Winkle

# TABLE OF CONTENTS

LIST OF ILLUSTRATIONS

LIST OF ILLUSTRATIONS (Cont'd)

LIST OF TABLES

SYMBOL TABLE

| | |
|---|---|
| $\alpha$ | phase variance |
| $\delta$ | Delta function |
| $\theta$ | angular measure |
| $k$ | wavenumber |
| $\lambda$ | wavelength |
| $\pi$ | 3.1416 |
| $\rho$ | density, correlation distance |
| $\sigma$ | standard deviation |
| $\tau$ | time variable |
| $\phi$ | angular measure |
| $\psi$ | angular measure ($k\sin\theta$) |
| $\delta$ | radian frequency |
| $\Delta$ | difference |
| $\Gamma$ | gamma function |
| $\Lambda$ | diffraction parameter |
| $\xi$ | variable |
| $\Phi_s$ | source function |
| $\Phi$ | strength parameter |
| $\Psi$ | wave functions |
| $\Omega$ | solid angle |
| $a$ | subscript signifying array |
| $c_o$, $c$ | speed of sound |
| $f$ | frequency |
| $i$ | index, $\sqrt{-1}$ |
| $k$ | wavenumber |
| $\ell_H$, $L_H$, $L_c$ | horizontal coherence length |

| | |
|---|---|
| $\ell_V$, $L_V$ | vertical coherence length |
| r, R | radial distance |
| t | time |
| y | spatial coordinate |
| x | spatial coordinate |
| m | intergers |
| n | intergers |
| o | subscript referring to incident arrival |
| $A_T$ | coefficient of the temperature power low spectrum |
| C | speed of sound |
| $C_\phi$, $C_\alpha$, $C_m$ | Correlation coefficients on $\phi$, x, m |
| $D_o$ | ideal gain |
| D(1,2) | structure function between points 1 to 2 |
| E, $E_\omega$, $E_f$ | Environmental parameters with $\omega$ and f |
| F, $F^{-1}$ | Fourier Transforms |
| G | Green's function |
| $I(C_m, \psi)$ | Shifrin's Parameterized Integral |
| L | Length |
| M | Interger |
| N | Interger |
| P | Pressure |
| **P** | Probability density function |
| R, $R_p$, $R_\phi$ | Normalized Correlations Functions |
| Q | Autocovariance function |
| $S(\psi)$ | line array wavenumber spectra |
| $S_p(\omega,k)$ | frequency-wavenumber spectra for pressure |
| T | Time, Temperature |

BWFN          Beamwidth Between First Nulls

HPBW          Half-Power Beamwidth

RSG           Relative Signal Gain

DASG          Differential Array Signal Gain

INTRODUCTION

This paper treats the subject of space-time processing and the application of ocean-acoustic arrays. Space-time processing has been extensively studied from a radar viewpoint since the forties and many comprehensive reviews and texts can be found. The Winder and Loda (1962)[1] summary of acoustic-space-time processing together with the fundamentals of statistical communication theory[2-5] provides a basis for the processing of ocean acoustic waves. The problem of the response of the acoustic antenna to a signal with random parameters was first treated by Bourret[6] followed by Berman[7] and Bordelon[8]. Additional work was performed by Brown[9] and Lord and Murphy[10] (also see ref 11). Shifrin[12] applied a similar approach to determine the statistical characteristics of radar antennas and his text treats in detail the response of antenna systems to waves with random amplitude and phase components. His results will be used as they apply to ocean acoustic arrays. Additional[13-17] reviews and texts stress the digital signal processing aspects of the problem. These include the use of digital Fast Fourier Transforms (FFT), shading characteristics,[14,15] and high resolution techniques.[15-17] These reviews for the most part address spatial and temporal processing separately but have direct application to sonar processing in space-time.

With such a formidable amount of previous papers, reviews, and texts, one may question the necessity for an additional paper on the subject. However, in underwater acoustics, the changes caused by multipath propagation and relative source-receiver motion through the severe acoustic interference field merit discussion. This paper utilizes the information available in the previous reviews[1-17] as applied to the characteristics of acoustic antennas in the mid-frequency range. The paper addresses aspects of the problem unique to

the acoustic antenna which result from the ocean environment and the acoustic field. It also treats the problems of measurement of the spatial coherence and the characteristic of linear arrays. Finally the paper discusses space-time processing when the temporal and spatial variables are weakly coupled.

## THEORETICAL BACKGROUND

This paper addresses the space-time processing of acoustic signals which satisfy the wave equation that in the absence of surfaces which scatter or diffract can be represented by:

$$\Box^2 \Psi(\underline{x},t) = -4\pi \Phi_s(\underline{x}_o,t_o)$$

$$\Psi(\underline{x},t) = \iiiint dt_o dV_o G(\underline{x},\underline{x}_o,t,t_o) \Phi_s(x_o,t) \qquad (1)$$

$$\Box^2 G(\underline{x},\underline{x}_o,t,t_o) = -4\pi\delta(\underline{x}-\underline{x}_o)\ \delta(t-t_o)$$

These solutions $(\Psi,G)$ are known to be continuous functions with continuous first derivatives. The solutions are also bounded by the imposition of a radiation condition at infinity. The solutions and the source function, $\Phi_s(x_o,t_o)$, usually have the property that the temporal and spatial characteristics are separable. Furthermore, the sources of sound of interest here are harmonic and have been excited for a time period sufficiently long that a steady state has been achieved. Since the acoustic pressure can be written as

$$P(\underline{x},t) = -\rho\ \partial\Psi(\underline{x},t)/\partial t \qquad (2)$$

and since superposition applies, the Dirichlet conditions are satisfied and Fourier analysis can be used to describe the space-time properties.

THE FOURIER TRANSFORM IN SPACE AND TIME

The pressure can be written as:[18]

$$P(\underline{x},t) = \frac{1}{(2\pi)^4} \iiiint F_p(\omega,\underline{k})\ \exp(i\omega t - i\underline{k}\cdot\underline{x})\ d\omega d^3\underline{k} \qquad (3)$$

and the frequency - wavenumber transform as:

$$F_p(\omega,\underline{k}) = \iiiint p(\underline{x},t)\ \exp(-i\omega t + i\underline{k}\cdot\underline{x})\ dt d^3 x \qquad (4)$$

This frequency-wavenumber transform contains the spatial and frequency characteristics of the acoustic pressure field. This transform is related to the space-time autocorrelation and correlation function of the acoustic pressure. The space-time correlation function is:

$$R_p(t_1,t_2,\underline{x}_1,\underline{x}_2) = \iiint P(\underline{x}_1,t) \ P^\dagger(\underline{x}_2,t_2) \ dt_2 d\underline{x}_2 \tag{5}$$

In the cases of a harmonic field which is steady or for a random field which is spatially homogeneous and temporally stationary, one can infer the space-time correlation function is only dependent on the relative separations in space and time.

$$R_p(t_1,t_2,\underline{x}_1,\underline{x}_2) = R_p(t_1,t_1+\tau,\underline{x}_o,\underline{x}_1+\underline{r}) = R_p(\tau,\underline{r}) \tag{6}$$

Furthermore, if an arbitrary functions is amenable to Fourier analysis, then according to the Wiener-Khintchine theorem the correlation function and the power spectra are Fourier transforms.[1-5] The frequency-wavenumber spectra is

$$S_p(\omega,\underline{k}) = \iiint R_p(\tau,\underline{r}) \ \exp[-i(\omega\tau-\underline{k}\cdot\underline{r})] \ d\tau d^3\underline{r} \tag{7}$$

and the correlation function

$$R_p(\tau,\underline{r}) = \frac{1}{(2\pi)^4} \iiint S_p(\omega,\underline{k}) \ \exp[i(\omega t-i\underline{k}\cdot\underline{r})] \ d\omega d^3\underline{k} \tag{8}$$

These relationships define the acoustic-space-time field for the class of harmonic and random functions which are spatially homogeneous and temporally stationary. These relationships show that when a narrowband characteristic exists in the frequency-wavenumber domain, i.e., a peaked distribution in $\omega$ and k, then the correlation function is broad in time $\tau$ and with respect to the spatial coordinate $\underline{r}$. In this case the field is termed spatially and temporal-

ly coherent. On the other hand, if the temporal correlation function is strongly peaked in $\underline{r}$ and $\tau$, then the frequency-wavenumber spectra is broad and the field is termed incoherent.

THE STATISTICAL REPRESENTATION

The usual method of determining the correlation function has been to use temporal averaging of the pressure field. An alternative method would be statistical averaging or the computation of the expectation value. The temporal representation is:

$$R_{pt}(\tau,\underline{r}) = \lim_{T\to\infty} \frac{1}{2T} \int_{-T}^{T} P(t,\underline{r})\ P^{\dagger}(t+\tau,\underline{r})\ dt = \langle P(t,\underline{r})\ P^{\dagger}(t+\tau,\underline{r}) \rangle \qquad (9)$$

and the statistical determination is:

$$R_{ps}(\tau,\underline{r}) = E\{P_1(t,\underline{r})\ P_2(t+\tau,\underline{r})\} = \iint_{-\infty}^{\infty} P_1 P_2\ \mathbf{P}(P_1,P_2)\ dP_1 dP_2 \qquad (10)$$

where $\mathbf{P}(P_1,P_2)$ is the joint probability density function for the ensemble of values $P_1$, $P_2$ and the process is a stationary one. The statistical computation $R_{ps}(\tau,\underline{r})$ is only equal to the temporal computation $R_{pt}(\tau,\underline{r})$ when the process is deterministic or ergodic. This is an important consideration in the comparison of space-time processes which are statistically computed and which are temporally measured. The statistical averaging corresponds to all the different states encompassed by the ensemble; however, the temporal averaging only corresponds to those states actually observed. Similar reasoning applies to the averaging over the spatial variable, $\underline{r}$. When the field is homogeneous and stationary, then (in large average limits) spatial and temporal average values approach the statistically determined expectation values.

THE SPACE-TIME TRANSFORM SUMMARY

The relationships between the space-time transforms has been discussed previously and can be summarized as follows:

# THE SPACE TIME TRANSFORMS

$$P(\underline{r},t) \xrightarrow{\quad F(P(\underline{r},t)) \quad} F_p(\omega,\underline{k})$$
$$\xleftarrow{\quad F^{-1}(F_p(\omega,\underline{k})) \quad}$$

$$\langle P_1(r_1,t) \cdot P_2^\dagger(r_2,t+\tau) \rangle \qquad\qquad F_p(\omega,\underline{k}) \cdot F_p^\dagger(\omega,\underline{k})$$

$$R_p(\tau,\underline{r}) \xrightarrow{\quad F(R_p(\tau,\underline{r})) \quad} S_p(\omega,\underline{k})$$
$$\xleftarrow{\quad F^{-1}(S_p(\omega,\underline{k})) \quad}$$
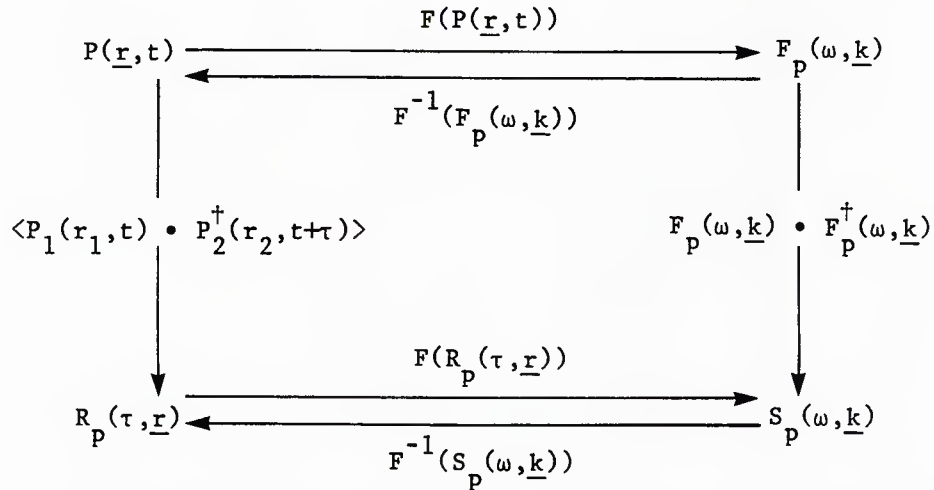
where $F$ and $F^{-1}$ refer to the Fourier transform and its inverse. These transformations are useful in the determination of the properties of the particular field $P(\underline{r},t)$ provided one can measure $S_p(\omega,\underline{k})$.

To describe the field $P(\underline{r},t)$ by the measurement of $S_p(\omega,\underline{k})$ one needs to account for the response of the measurement system. If this response is designated by $f(\underline{r},t)$ which describes the spatial and temporal response of the system and $F_{mp}(\omega,\underline{k})$ represents the measured transform

$$F_{mp}(\omega,\underline{k}) = F\{f(\underline{r},t)\, P(\underline{r},t)\} = F\{f(r,t)\} * F\{P(\underline{r},t)\} = f_{1p} * F_p \qquad (11)$$

where $*$ refers to convolution.

Thus the frequency-wavenumber spectra is the convolution of the transform of the system response and the transform of the field. This is a very useful

concept as it allows one to consider the system response and its Fourier transform independent of the acoustic field variables. Furthermore, since

$$S_{mp}(\omega,\underline{k}) = F_{mp}(\omega,\underline{k})\ F_{mp}^{\dagger}(\omega,k) \tag{12}$$

represents the output of the system, one concludes that broadness in the system response function $f_{\ell p}(\omega,\underline{k})$ and broadness in acoustic wavenumber spectra both determine the broadness of $S_{mp}(\omega,\underline{k})$. This concept implies that in the spatial domain, the broadness of $f_{\ell p}(\omega,\underline{k})$ with respect to $\underline{k}$ is determined by the shading characteristic and length of the system. Matched processing would require that the spread of $\underline{k}$ for both $f_{\ell p}(\omega,\underline{k})$ and $F_{p}(\omega,\underline{k})$ would be equal. Recall that the angular spread in $F_{p}(\omega,\underline{k})$ is caused by the environment.

SYSTEM RESPONSE

The description of the system response can easily be developed by the direct analogy between sampling in time and sampling in space. Since the developments elsewhere concentrate on the time domain, this paper will proceed with a spatial description of the system response. The particular case of a one-dimensional linear sample, a line array, is described by the illumination function, shading, or window function. Several representative window functions are shown in Figure 1 based on the integral form of the Fourier transform. The rectangular window transform follows directly from equation 4. Neglecting the time-frequency transform, one has

$$f_{\ell p}(\underline{k}) = \int_{-a/2}^{a/2} f(x)\ \exp(ikx)\ dx = a\ \sin\ (ak/2)/ak/2 \tag{13}$$

the result is the same whether the sampling is in space or in time. For the case of discrete elements within the array we have
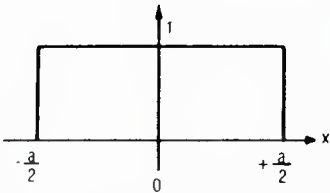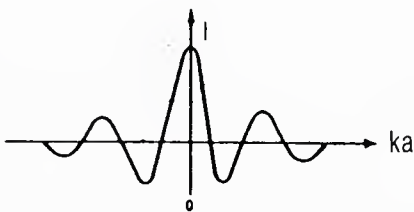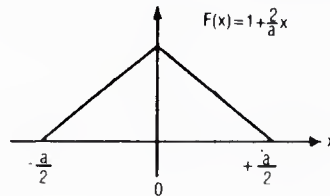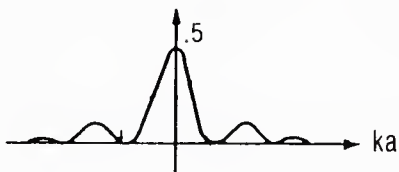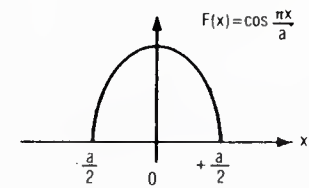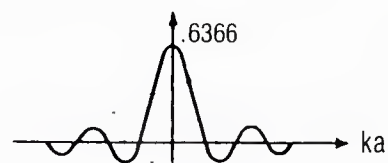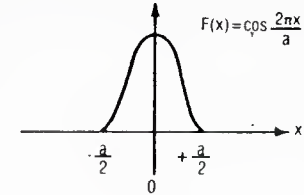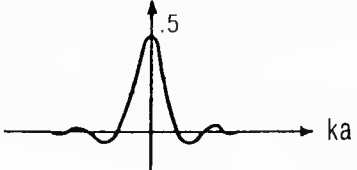
| WAVEFORM | F(x) | $f_{lp}(k)$ | |
|---|---|---|---|
| CONSTANT |  |  | $\dfrac{f_{lp}(k)}{a} = \dfrac{\sin(ka/2)}{ka/2}$ |
| TRIANGULAR |  $F(x) = 1 + \frac{2}{a}x$ |  | $\dfrac{f_{lp}(k)}{a} = \dfrac{1}{2} \cdot \left(\dfrac{\sin(ka/4)}{ka/4}\right)^2$ |
| COSINE |  $F(x) = \cos\frac{\pi x}{a}$ |  | $\dfrac{f_{lp}(k)}{a} = \dfrac{\pi}{a} \cdot \dfrac{\cos(ka/2)}{(\pi/2)^2 - (ka/2)^2}$ |
| COSINE SQUARED |  $F(x) = \cos\frac{2\pi x}{a}$ |  | $\dfrac{f_{lp}(k)}{a} = \dfrac{1}{2} \dfrac{\sin(ka/2)}{ka/2} \dfrac{\pi^2}{\pi^2 - (ka/2)^2}$ |

Figure 1. Window functions determined from the Fourier integral for finite apertures.

$$f_{\ell p}(k) = \int \sum_{n=1}^{N} \delta(x - nd)\exp(ikx)dx = \frac{\sin(Nk_o d\sin\theta)}{N\sin(k_o d\sin\theta)} \tag{14}$$

This result agrees closely with the continuous line array (equation 13) when the spacing is half wavelength ($d = \lambda/2$) as shown in Figure 2.[1] The window factors listed in Table 1 are taken from Harris's[14] concise review of discrete Fourier transforms and the use of windows. For the purpose of this paper we will continue with the integral (continuous) description of the transform, recognizing that small differences do exist.
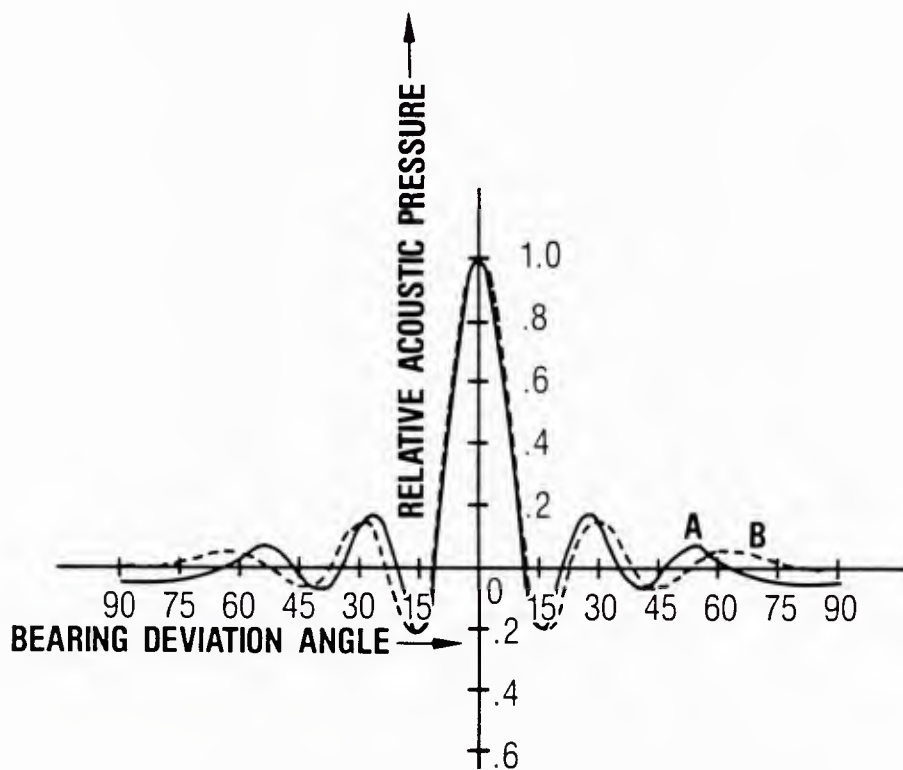


Figure 2. A comparison of the directivity patterns of (a) a discrete linear array having elements spaced at half wavelengths and (b) a continuous, uniform line transducer.

Table 1.  Representative window function in properties after Harris (1978)[14]

| WINDOW | HIGHEST SIDELOBE LEVEL (dB) | SIDELOBE FALLOFF (dB / OCT) | COHERENT GAIN | EQUIV. NOISE. BW (BINS) | 3.0-dB BW (BINS) |
|---|---|---|---|---|---|
| Dirichlet. rectangle | -13 | -6 | 1.00 | 1.00 | 0.89 |
| Fejer triangle | -27 | -12 | 0.50 | 1.33 | 1.28 |
| cos $\alpha$ [X]    $\alpha = 1.0$<br>Hann      $\alpha = 2.0$<br>         $\alpha = 3.0$<br>         $\alpha = 4.0$ | -23<br>-32<br>-39<br>-47 | -12<br>-18<br>-24<br>-30 | 0.64<br>0.50<br>0.42<br>0.38 | 1.23<br>1.50<br>1.73<br>1.94 | 1.20<br>1.44<br>1.66<br>1.86 |
| Hamming | -43 | -6 | 0.54 | 1.36 | 1.30 |
| Tukey<br>(cosine<br>tapered) | -14<br>-15<br>-19 | -18<br>-18<br>-18 | 0.88<br>0.75<br>0.63 | 1.10<br>1.22<br>1.36 | 1.01<br>1.15<br>1.31 |
| exp$(-\alpha X)$   $\alpha = 2.0$<br>Poisson   $\alpha = 3.0$<br>         $\alpha = 4.0$ | -19<br>-24<br>-31 | -6<br>-6<br>-6 | 0.44<br>0.32<br>0.25 | 1.30<br>1.65<br>2.08 | 1.21<br>1.45<br>1.75 |
| Hann-     $\alpha = 0.5$<br>Poisson   $\alpha = 1.0$<br>         $\alpha = 2.0$ | -35<br>-39<br>NONE | -18<br>-18<br>-18 | 0.43<br>0.38<br>0.29 | 1.61<br>1.73<br>2.02 | 1.54<br>1.64<br>1.87 |
| Cauchy<br>$\left[ \dfrac{1}{1+(\alpha X)^2} \right]$   $\alpha = 3.0$<br>$\alpha = 4.0$<br>$\alpha = 5.0$ | -31<br>-35<br>-30 | -6<br>-6<br>-6 | 0.42<br>0.33<br>0.28 | 1.48<br>1.76<br>2.06 | 1.34<br>1.50<br>1.68 |
| Gaussian    $\alpha = 2.5$<br>exp$(-\alpha^2 X^2/2)$ $\alpha = 3.0$<br>           $\alpha = 3.5$ | -42<br>-55<br>-69 | -6<br>-6<br>-6 | 0.51<br>0.43<br>0.37 | 1.39<br>1.64<br>1.90 | 1.33<br>1.55<br>1.79 |
| Dolph-<br>Chebyshev | -50<br>-60<br>-70<br>-80 | 0<br>0<br>0<br>0 | 0.53<br>0.48<br>0.45<br>0.42 | 1.39<br>1.51<br>1.62<br>1.73 | 1.33<br>1.44<br>1.55<br>1.65 |
| Kaiser-<br>Bessel | -46<br>-57<br>-69<br>-82 | -6<br>-6<br>-6<br>-6 | 0.49<br>0.44<br>0.40<br>0.37 | 1.50<br>1.65<br>1.80<br>1.93 | 1.43<br>1.57<br>1.71<br>1.83 |

RESOLUTION

The reciprocal relationship between aperture and beam width can easily be seen by examination of the results from the rectangular window.

$$F_{\ell p}(k,\omega_o) = Lsin(kL/2)/kL/2 = Lsin(\pi Lsin\theta/\lambda)/\pi Lsin\theta/\lambda \qquad (15)$$

The radiation pattern (here we use the principle of reciprocity) is simply $F_{\ell p}(k,\omega_o) \ F_{\ell p}^{\dagger}(k,\omega_o)$ and represents the Farfield radiation pattern sometimes referred to as the Fraunhofer region as opposed to Fresnel and nearfield regions.

$$F_{\ell p}(k,\omega_o) \ F_{\ell p}^{\dagger}(k,\omega_o) = L^2sin^2(\pi Lsin\theta/\lambda)/(\pi Lsin\theta/\lambda)^2 \qquad (16)$$

The result is as expected; that for a perfectly coherent incident field an increase in antenna length results in additional power output and a reduction in beam width. These effects are illustrated in Figure 3 for both space L and time T.
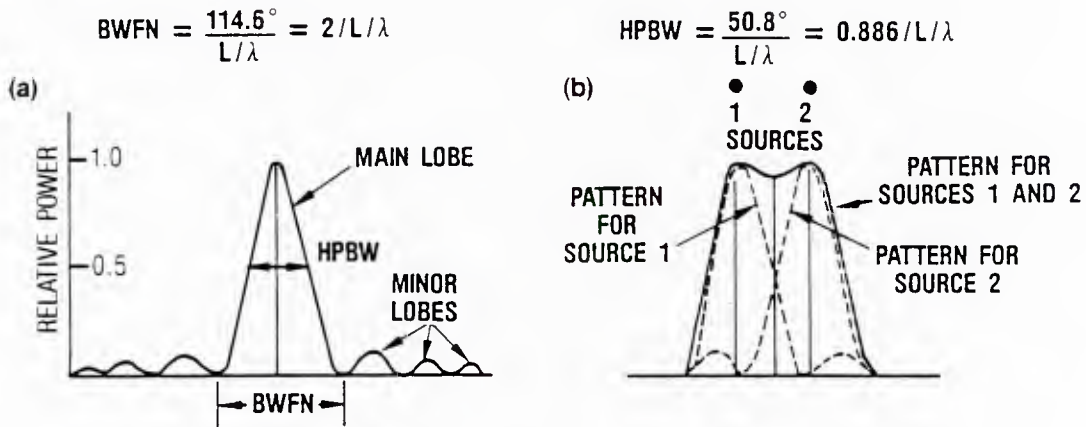


Figure 3.  (a) Power pattern and (b) power patterns for two identical point sources separated by the Rayleigh angle as observed individually (dashed) and together (solid).

The resolution relationship can be explored by a variety of criteria. Lord Rayleigh's Criterion (1897)[19] was the resolvability of two sources when the maximum of the pattern for one coincided with the first minimum of the other. This corresponds to one half the beam width between first nulls (BWFN)

$$\text{Rayleigh Resolution Criteria } R = BWFN/2 \qquad (17)$$

The first null occurs when:

$$\pi L \sin\theta/\lambda = \pi; \quad L\sin\theta/\lambda = 1 \qquad (18)$$

The beamwidth between the first nulls would then be:

$$\Delta\theta_{FN} = 2\lambda/L \qquad (19)$$

The alternative description also shown in Figure 3 is to choose the half power (hp) points which can be seen to be:

$$\Delta\theta_{hp} = 0.886 \, \lambda/L; \quad R = \lambda/L = \Delta\theta_{FN}/2 = 1.12 \, \Delta\theta_{hp} \qquad (20)$$

This relationship holds for the broadside case of the spatial array and can be generalized for the off broadside and end fire cases as follows:

$$\text{Near Broadside} \qquad \Delta\theta \cdot L/\lambda = 0.886 \, \sec\theta_o \qquad (21)$$

however

$$\text{Near End Fire} \qquad \Delta\theta(L/\lambda)^{1/2} = 2(0.886)^{1/2} \qquad (22)$$

this is simply a consequence the properties of the trigonometric relations. The relations indicated here are applicable to other window functions such as those shown in figure 1 and can be found in Harris[14] as shown in table 1. The major conclusion drawn here is that in general

$$\Delta\theta \cdot L/\lambda = C_\ell \simeq 1 \qquad (23)$$

$$\Delta f \cdot \Delta t = C_t \simeq 1 \tag{24}$$

represents the resolution properties of space-time processors.

These results are based solely on the deterministic response of the line array. However, as was mentioned before in connection with equation 11, one must require that the resolution of the system be less than or equal to the angular spread in the incident field. Equation 11 shows that the measured output is the convolution of the system response and the field frequency-wavenumber transform. In an analogous fashion, one can relate the output of the measurement system as the convolution of the array response $f_{\ell p}(k,\omega)$ and the Fourier transform of the acoustic spatial correlation function

$$S_p(k\sin\theta,\omega) = f_{\ell p}(k\sin\theta,\omega) * F(R_p(\underline{r},\tau)). \tag{25}$$

The acoustic spatial correlation function, when we have suppressed the temporal variables, can also be defined as

$$R_p(\underline{r}_1, \underline{r}_2) = \{p(\underline{r}_1) \, p^{\dagger}(r_2)\} \tag{26}$$

where $\underline{r}_1$ and $\underline{r}_2$ are the spatial location points, p is the complex acoustic pressure, † indicates conjugation, and the braces indicate ensemble averaging. The relationship between $R_p$ and the receiving array beam power output s is shown in equation 27 for the case of standard beamforming in an acoustic field that is homogeneous across the receiver:

$$S(k\sin\theta) = \int f_{\ell p}(k\sin\theta - k\sin\theta') \{ \int R_p \exp(-ik\sin\theta' r)dr \} \, d(k\sin\theta')$$

$$= f_{\ell p} * F(R_p) \tag{27}$$

In this case the array output as a function of horizontal angle $\theta$ is simply the convolution of the array beam pattern $f_{\ell p}$ with the angular distribution

of incoming acoustic signals, which is given by the spatial Fourier transform
F of the acoustic correlation function. The symbol $\underline{k}$ is the acoustic wavenumber at the receiver, and the Fourier transfom is taken with respect to the spatial coordinate $\underline{r}$.

In long range propagation cases, it is expected that the initially smooth curve wave fronts, in the ray theory sense, will have become irregular and spatially varying descriptions of forward scattered energy bundies. These "arrivals" are resolvable in order but, when displayed after suitable steering delays, have a phase and amplitude variability as well as extended durations greater than the transmitted pulse. These distorted pulses decorrelate in space--a phenomenon equivalent to an angular redistribution of energy.

The effects of disparities between the array properties and the incoming signal angular distribution are immediately apparent from equation 27. A short array with a beam pattern broader than the signal angular distribution is accepting unnecessary noise on the main lobe, whereas a long array with a beam pattern narrower than the signal angular spread is rejecting part of the power in the signal. Thus, the design of optimal array characteristics is facilitated by a prior knowledge of the acoustic correlation function.

The angular spread of arriving acoustic waves during a given observation period can also be due to the arrival of multiple rays at different angles. That is to say, off broadside arrivals from the same azimuthal angle but with different vertical arrival angles can have conical angles such that the difference between the conical angles from multiple rays is greater than the half power beamwidth of the array. Thus one will observe a bifurcation or the appearance of acoustic intensity on more than one beam. The angle of arrival for a given path or group of paths depend on the relative orientation and

motion between the source and receiver during the observation period. Consequently, motion both radially and with respect to relative azimuth can have a smearing effect on the beam response. This phenomena of coupling between the angular spread and the relative source-receiver motion is treated later in the paper.

An analogous situation exists for the frequency domain. Spread in the frequency domain can be caused by random media scatter, doppler spread due to multipath projections of radial velocity and accelerations. The doppler spread due to the relative motion source receiver is normally the dominant effect and the remaining causes of frequency spread are small.

## STATISTICAL CHARACTERISTICS[12]

The determination of the response of an array to a signal with variability in phase is of major importance to our discussions. The following treatment of the response of a continuous line array to a random signal closely follows the derivation of Shifrin[12] and is included here because the results do not appear to be used extensively in acoustic antenna applications despite some previous results worthy of note.[6-11] Starting with the transform of a uniform line array of length L illuminated by a harmonic wave p(y) where the time dependence is suppressed, one has

$$f_{\ell p}(k\sin\theta) = \int_{-L/2}^{L/2} P(y)\exp\{iky\sin\theta\}dy \tag{28}$$

for convenience, we let

$$\psi = \pi L\sin\theta/\lambda \text{ and } x = 2y/L$$

$$f(\psi) = f_{\ell p} \cdot 2/L = \int_{-1}^{+1} P(x)\exp(i\psi x)dx \tag{29}$$

The pressure field p(x) is assumed to have a phase $\phi(x)$ which is a zero mean random variable with a Gaussian correlation function.

$$P(x) = P_o\exp(i\phi x), \quad \overline{\phi}(x) = 0, \quad \overline{\phi^2}(x) = \sigma_\phi^2 = \alpha \tag{30}$$

$$R_\phi = \frac{\overline{\phi(x_1)\,\phi(x_2)}}{\sigma_\phi(x_2)\,\sigma_\phi(x_2)} = \exp\{-(x_1 - x_2)^2/C_\phi^2\}, \quad C_\phi = 2\rho/L \tag{31}$$

upon substitution one has

$$f(\psi) = \int_{-1}^{+1} P_o\exp\{i\phi(x) + i\psi x\}dx \tag{32}$$

The quantity $f(\psi)$ is the spatial wavenumber transform of the field. One can compute the mean wavenumber transform and the power wavenumber spectra (which is completely analogous with the farfield-power-radiation pattern of an antenna with variable current drive within the aperture). These computations provide the basis for the determination of the role the variance $(\sigma_\phi^2 = \alpha)$ and the correlation length $(C_\phi = 2\rho/L)$ have on the measured antenna characteristics. Since the process is a stationary Gaussian process, the averaging will be ensemble averaging. The mean field is

$$\left|\overline{f(\psi)}\right| = \int_{-1}^{+1} P_o\exp\{\overline{i\phi(x)} + i\psi x\}dx = \int_{-1}^{+1} P_o\exp\{\frac{-\sigma_\phi^2}{2} + i\psi x\}dx$$

$$= P_o\exp\left(\frac{-\sigma_\phi^2}{2}\right)\frac{\sin\psi}{\psi} \tag{33}$$

The important determination of the quantity $\exp(\overline{i\phi(x)})$ is from the characteristic function for a Gaussian distribution and can be found in references 2, 3, 8 and 12. Similarly one has for the farfield pattern, again using reciprocity,

$$\left|\overline{f(\psi)}\right|^2 = \iint_{-1}^{+1} P_o(x)P_o(x_1)\exp\{\overline{i(\phi(x)-\phi(x_1))}\}\exp(i\psi(x-x_1))dxdx_1 \tag{34}$$

This integral can be simplified for both the Gaussian and exponentially distributed random variables. This paper will simply outline the approach for the Gaussian case as presented by Shifrin.

$$|\overline{f(\psi)}|^2 = \iint_{-1}^{+1} P_o^2 \exp\{\alpha R_\phi - \alpha + i\psi(x - x_1)\}dxdx_1 \qquad (35)$$

where

$$\alpha = \sigma_\phi^2, \quad R_\phi = \exp\{-(x - x_1)^2/C_\phi^2\}, \quad C_m = C_\phi/\sqrt{m} = 2\rho/\sqrt{m}L \qquad (36)$$

$$\exp(\alpha R_\phi) = 1 + \sum_{m=1}^{\infty} \frac{\alpha^m}{m!} \exp\{-(x - x_1)^2/C_m^2\}$$

then

$$|\overline{f(\psi)}|^2 = \exp(-\alpha)\{P_o^2 \iint \exp(i\psi(x-x_1))dxdx_1 +$$

$$\sum_{m=1}^{\infty} \frac{\alpha^m}{m!} P_o^2 \iint_{-1}^{+1} \exp\left(\frac{-(x-x_1)^2}{C_m} + i\psi(x-x_1)\right) dxdx_1 \qquad (37)$$

finally with $P_o = 1/2$ one has

$$|\overline{f(\psi)}|^2 = \exp(-\alpha)\{\frac{\sin^2 \psi}{\psi^2} + 1/4 \sum_{m=1}^{\infty} \frac{\alpha^m}{m!} I(C_m,\psi)\} \qquad (38)$$

The mean power pattern has thus been shown to depend on the pattern in the absence of phase randomness and a distortion in the pattern due to the combined influence of the phase variance $\alpha$ and the normalized correlation length, $C_m$. The power in the direction of the principal maxima is also seen to be decreased by the factor $\exp(-\alpha)$. The function $I(C_m,\psi)$ can be evaluated in closed form for special cases. A similar function can be derived when the exponential form of the correlation function is used.

The figure 4 from Shifrin shows the mean power radiation pattern $|\overline{f(\psi)}|^2$ versus the angle $\psi$ for various values of the phase variance $\alpha$ and the normalized correlation length C. These calculations by Shifrin show some interesting general characteristics. The randomicity in phase quantified by the variance shows that the effect of an increase causes the principal maxima to decrease (see a, b, c, d and e). In addition, the phase variance results in a smoothing or smearing of the radiation pattern, that is, the nulls are filled or blurred. As the phase variance increases, the pattern loses detailed structure and becomes a monatonically decreasing one (see a and b for $\alpha = 3$). The effect of increasing the phase correlation length is shown in figure 4e. As C increases, the pattern approaches the ideal pattern, the power in the direction of the principal maxima increases (see example e and f). In summary, the increase in phase variance causes a reduction in power for the principal maxima and a blurring of the pattern. An increase in the phase correlation length causes the power for the principal maxima to increase and the pattern to approach the ideal case. These were numerical computations performed by Shifrin. The expression can be simplified to approximate forms as discussed next.

When the correlation distance of the phase fluctuations is sufficiently great to make the variation in phase over a wavelength along the array small with respect to unity then the mean directional gain can be shown to be

$$\overline{D} = P_o \exp(-\alpha)\{1 + 1/4 \sum_{m=1}^{\infty} \frac{\alpha^m}{m!} I(C_m, 0)\} \tag{39}$$

It is instructive to consider the behavior of D when the length of the array (L) is much smaller than the correlation distance ($2\rho \gg L, C > 1$). We can further divide this case into two regions. Region I where $C/\sqrt{\alpha} = 2\rho L/\sqrt{\alpha} > 1$ and region II where $C/\sqrt{\alpha} < 1$.
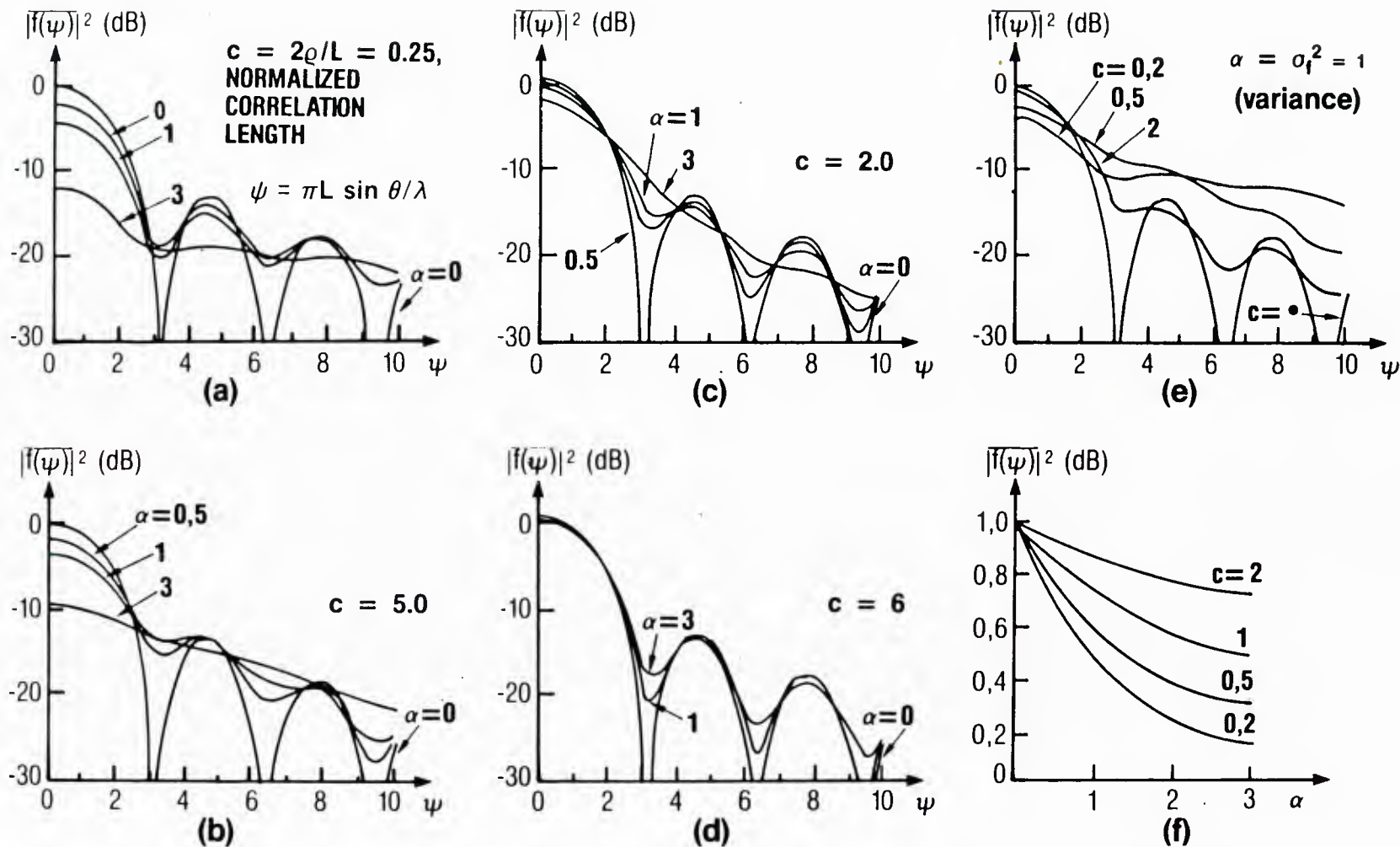
Figure 4. The mean radiation pattern $|\overline{f(\psi)}|^2$ for various values of the phase variance ($\alpha = \sigma_\phi^2$) and the phase correlation length ($C_m = 2\rho/\sqrt{mL}$) versus $\psi = \pi L \sin\theta/\lambda$. (a-d) show the mean radiation pattern of a linear system for various $\alpha$ with (a) C = 0.25, (b), C = 0.5, (c) C = 2.0, (d) C = 6.0. For all values of C the effect of $\alpha$ is to decrease the intensity at the principal maximum and to smooth the pattern by filling the nulls. (e) shows for a constant $\alpha$, the efffect of increase in phase correlation length on the character of the pattern while (f) shows for constant correlation length the effect of phase variance increase on the principal maximum.

In the first region, figure 5, the mean directional gain can be shown to be

$$C/\sqrt{\alpha} > 1, \quad \overline{D} = D_o I(C_\alpha, 0) = D_o(1 - 2\alpha/3C^2) \simeq D_o \tag{40}$$

which is equal to the ideal gain of the line array. In the second region, the directional gain can be approximated by

$$C/\sqrt{\alpha} < 1, \quad \overline{D} = D_o I(C_\alpha, 0)/4 \simeq D_o \sqrt{2\pi} \, C/4\sqrt{\alpha} \simeq 2\sqrt{\pi/\alpha}(\rho/\lambda) \tag{41}$$

This expression shows the mean directional gain to be independent of array lengths, i.e., saturated.
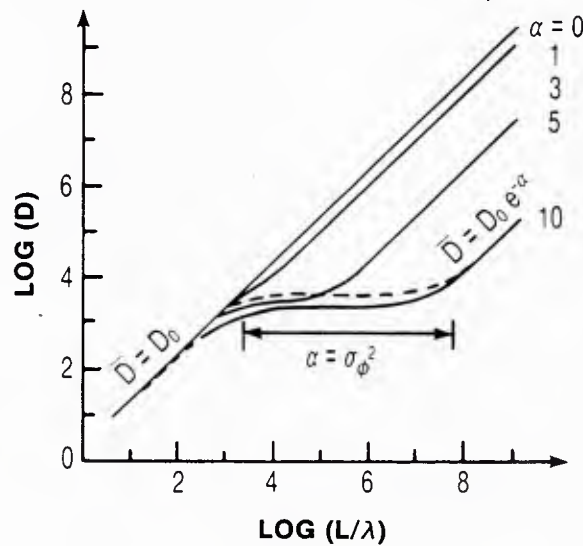


Figure 5. Mean directive gain versus length $(L/\lambda)$.

One may interpret these results by considering the relationship between the phase variance $\alpha = \overline{\Delta\phi^2}$ and the variance of the arrival angle $\theta$ of the acoustic wave with respect to the array. Since $\rho > L$, the mean phase variation across the array may be taken as $\overline{\Delta\phi} = kL\overline{\theta}$. For this case of $\rho > L$ we have for

the Gaussian variable $\overline{\Delta\phi^2} = 2\alpha L^2/\rho^2$. Equating these quantities leads to the result for the mean square variation in the arrival angle $\theta$ to be

$$\overline{\theta^2} = 8(\sigma_\phi L/\rho)^2/k^2 L^2 = 8(\sqrt{\alpha}/c)/k^2 L^2 \qquad (42)$$

Then this estimate of the angular spread in the acoustic field can be compared to the half-power width of the antenna pattern.

$$\Theta_{hp} = 2\theta_{hp} \simeq \lambda/L; \quad (C/\sqrt{\alpha})^2 = 2\Theta_{hp}/(\pi\theta)^2 \qquad (43)$$

When $\Theta_{hp} < \overline{\theta^2}$ then the spread in the angle of the incident energy is greater than the half-power beam width and $C_\alpha < 1$. In this instance, our antenna exhibits saturation. On the other hand, when $\Theta_{hp} > \theta^2$, the beam width of the antenna is greater than the incident spread of energy and an increase in length results in an increase in mean directional gain.

The final case is when the length of the antenna is much greater than the correlation length ($L > \rho$, $c < 1$). In this instance, equation 39 for the mean directive gain becomes ($I(C_m,0) \rightarrow 2\pi c/\sqrt{m}$)

$$\overline{D} = D_o \exp(-\alpha)\{1 + \frac{2C\sqrt{\pi}}{4} \sum_{m=1}^{\infty} \frac{\alpha^m}{m!\sqrt{m}}\} = D_o \exp(-\alpha)\ (1 + CN(\alpha)) \qquad (44)$$

when $CN(\alpha) > 1$, this term dominates the gain and since $(\overline{D} = D_o \exp(-\alpha)CN(\alpha) = 4\rho\exp(\alpha)N(\alpha)/4 = \overline{D}$ is again independent of array length, the array is still saturated. In the case of radar waves in the atmosphere, Shifrin maintains that further increases in the length of the system produces a point where $CN(\alpha) < 1$ and then the mean directive gain becomes $\overline{D} = D_o e^{-\alpha}$. That is although reduced by the constant factor $e^{-\alpha}$ the mean directive gain increases in proportion to the ideal gain, $D_o = 2L/\lambda$. This region III which is dominated by the correlation length is shown on figure 5. The existence of a region III for the

non-plane multipath underwater acoustic propagation case is still questionable. For wavelengths greater than 1.5 m, practical measurements in the ocean will be limited to $\log(L/\lambda) \leq 4$. The region II can be bounded by letting the approximate expression for $CN(\alpha) = 1$. When this is done, one arrives at an upper bound of region II

$$L_u = \sqrt{\pi} \, \rho \sum_{m=1}^{\infty} \alpha^m / m! \sqrt{m} \qquad \text{(45a)}$$

and the lower bound of region II

$$L_\ell = 2\rho / \sqrt{\alpha} \qquad \text{(45b)}$$

Thus the array behavior can be characterized provided one has a knowledge of $\alpha$ and $\rho$.

In summary, the presence of phase randomicity was shown to have marked effects on the mean radiation pattern and mean directive gain. The variance was found to cause a blurring of the pattern, i.e., the nulls are blurred and the principal maxima decreases. As the variance increases further the pattern was shown to become a monatonically decreasing function. As the correlation distance was increased the pattern was found to approach the characteristic of a system without phase fluctuations. The mean directional gain was shown to exhibit three types of behavior: the first, a region in which the gain increases proportional to $2L/\lambda$; the second, a region of gain saturation (gain independent of length); and the third, in which the gain increase by $2L/\lambda$ attenuated by $\exp(-\alpha)$. (This is questionable for long range underwater acoustic propagation.) These results were derived for a Gaussian correlation function but could also be developed for an exponential distribution.

In closing this section, the Gaussian correlation function is related to the measure of spatial coherence. Recalling equations 30, 31, and 35, one can indicate this relationship by noting

$$R_\phi = \exp\{-(x - x_1)^2/C_\phi{}^2\} \simeq 1 - |x - x_1|^2/C^2 \tag{46}$$

substitution of this quantity into equation 35 results in

$$|\overline{f(\psi)}|^2 = \iint_{-1}^{+1} P_o^2 \exp\{-(x - x_1)^2/C^2/2\lambda\}\exp(i\psi(x - x_1)) \, dxdx_1 \tag{47}$$

one recognizes $P_o^2 \exp(-(x-x_1^2)/L_H^2)$ as a Gaussian form of the spatial coherence function.

## COHERENCE

The statistical response of an array has been developed for a signal with a random component of phase which is Gaussian. Due to general characteristics of the Gaussian process, it can be shown that a random phase variable with a Gaussian spatial correlation function also produces a spatial coherence function which was found to have a Gaussian form. Although not shown in this paper, the random phase variable with an exponential correlation function produces an exponential spatial coherence function. The results have primarily dealt with the spatial dimension but also apply to the temporal scale.

The analogous nature of the treatment of coherence in space and time is restated in Figure 6. The top set of expressions the spatial coherence whereas the bottom sets describe the temporal coherence.

## SPATIAL COHERENCE

$$R_p = \langle P(X) \ P^*(X + R) \rangle \quad \text{Mutual coherence function}$$

$$F_S \{R_p\} \quad \text{Incident signal angular distribution}$$

$$S(k \sin \theta) = B_A \star F_S \{R_p\} \quad \text{Array beam signal output}$$

## TEMPORAL COHERENCE

$$Q = \langle P(T) \ P^*(T + \tau) \rangle \quad \text{Autocovariance function or fluctuation time series}$$

$$F_T \{Q\} \quad \text{Incident signal frequency spectrum}$$

$$S(\omega) = W \star F_T \{Q\} \quad \text{Processor signal output}$$

Figure 6. Spatial and temporal coherence relationships.

The top equation defines the spatial covariance of the acoustic field, $R_p$, to be the average of the product of the complex pressure at one point in the space domain with the complex conjugate of the pressure at a second point in space. In a number of theories for wave propagation in a random medium, this expression is called the mutual coherence function. The spatial Fourier transform of the mutual coherence function gives the incident signal angular distribution. It was shown for the case of standard beamforming and an acoustic field that is homogeneous across the aperture that the array beam signal output, $S(\omega,k)$, is the convolution between the array beam pattern and the incident signal angular distribution.

The bottom set of expressions treats temporal coherence. The first equation defines the temporal autocovariance function, Q, as the average of the product of the complex pressure at one point in time with the complex conjugate of the pressure at another point in time. This is sometimes referred to as the autocovariance function for the fluctuation time series. The temporal Fourier transform of Q gives the incident signal frequency spectrum. It can be shown that the processor signal output is the convolution of the processor spectral window with the incident signal frequency spectrum.

SPATIAL COHERENCE

The propagation of waves though a random media has been treated by Chernov[20] and Tatarski[21]. The results of Chernov's work and the experimental measurements discussed by Shifrin[12] were the basis for Shifrin's choice to use exponential and Gaussian phase correlation functions to determine the statistical characteristics of antennas. The Gaussian form was chosen to illustrate the general characteristics of line array when the incident wave had a normally distributed phase variable with a Gaussian correlation function. The exponen-

tial correlation function was not chosen, even though in several instances this function compares favorably with experimental data on electromagnetic propagation in the atmosphere, since an exponential correlation function represents a discontinuous physical process. The results of this treatment starting with the Gaussian phase correlation function were shown to produce an equivalent result with a Gaussian spatial coherence function (see eq. 47).

The ocean acoustics wave propagation problem is thought to be more complex than atmospheric propagation due to the spatial properties which are anisotropic and nonhomogeneous. A thorough discussion of this subject is beyond the scope of this paper and we refer the reader to some very excellent reviews.[22-27] (This subject has been extensively studied and comprehensively reviewed by Flatte.[22,23] Desaubies[25] has prepared a readable overview while McCoy[26] and Guthrie[27] have reviewed the work performed at the Naval Research Laboratory.)

We have shown that the output of a line array can be written as

$$S(\psi) = f_{\ell p}(\psi - \psi_o) * F(R_p) \tag{50}$$

The spatial coherence function as shown in figure 6 can be written as

$$R_p = \langle P(\underline{x}) \, P^{\dagger}(\underline{x} + \underline{r}) \rangle = \langle P^2 \rangle \exp(-(y/L_H)^n) \quad n = 1, \, 1.5, \, 2 \tag{51}$$

Where $\langle P^2 \rangle$ is the mean square pressure and is proportional to the acoustic intensity and where $n = 1$ is the exponential form, $n = 1.5$ the Beran-McCoy form, and $n = 2$ the Gaussian form. Since our goal is to understand line array performance in the linear region of figure 5 to the beginning of the gain saturation region, these types of coherence functions can be considered valid. Flatte[22,23] and Dashen[24] relate the coherence to a phase structure function.

$$R_p = <P^2> \exp(-D(1,2)/2) \tag{52}$$

and in the region of interest here, the geometrical acoustics and partially saturated ($\Phi\Lambda \simeq 1$) regions, they give the structure function at small separations to be

$$D(1,2) \simeq \Phi^2\{(T/\tau)^2 + (y/L_H)^2 + (Z/L_V)^2(\text{Log}(Z/L_V) + \Gamma_V)\} \tag{53}$$

The characteristic time $\tau = 1.6$ hours; the characteristic vertical coherence length, $L_V$, is 300 m; and the characteristic horizontal coherence length, $L_H$, is 3.7-6.4 km. The structure function given here clearly corresponds to a coherence function with $n = 2$, the Gaussian form.

The exponential functional form of the coherence was employed by Cox[28] since it enabled the development of a closed form solution to the array gain problem. Cox used the function only for small ($\lambda/2$) separations and the result is useful. However, as Shifrin has pointed out, this functional form has a finite derivative at zero separations and corresponds to a discontinuous physical process, not representative of wave propagation.

The work presented in this paper is based on the $n = 1.5$ functional form after the work of Beran and McCoy.[29,30]

Theoretical predictions for the acoustic correlation function can be obtained by solution of a Bethe-Salpeter equation that includes multiple scattering and the effects of random oceanic fluctuations:

$$R_p(\underline{x}_1, \underline{x}_2) = R_{p_o}(\underline{x}, \underline{x}_0)$$

$$+ \iint G(\underline{x}_2,P) \, k^2(\underline{\rho}) \, G(\underline{\rho},\underline{\rho}') \, k^2(\underline{\rho}') \, R_\varepsilon(\underline{\rho},\underline{\rho}') \, R_p(\underline{x},\underline{\rho}) d\rho \, d\rho' \tag{54}$$

$$+ \iint G(x_1,\underline{r})\ k^2(\underline{r})\ G(\underline{r},\underline{r}')\ k^2(\underline{r}')\ R_\epsilon(\underline{r},\underline{r}')\ R_p(r',x_2)drdr'$$

$$+ \iint G(\underline{x}_1,\underline{r})\ k^2(\underline{r})\ G(\underline{x}_2,\underline{\rho})\ k^2(\underline{\rho})\ R_\epsilon(\underline{r},\underline{\rho})\ R_p(\underline{r},\underline{\rho})drd\rho$$

The Bethe-Salpeter equation (Frisch (1968))[31] given in equation 54 is appropriate for a weak environmental-fluctuation field and is truncated at the two-point moment of the environment fluctuation. This integral formulation indicates that the acoustic correlation function at the receiver is a function of the following: $R_{p_o}$, the correlation function of the solution of the reduced deterministic wave equation; G, the Green's function for the reduced deterministic wave equation; $\underline{k}$, the deterministic wavenumber; $R_\epsilon$, the two-point correlation function for the random portion of the wavenumber; and $R_p$, the acoustic correlation function in the space between the source and receiver.

Four of the usual assumptions made to provide tractability to equation 54 are that (1) G is the infinite space Green's function; (2) the variation of the deterministic wavenumber is parametric with range; (3) the acoustic field is statistically homogeneous over distances that are large compared with the receiver aperture; and (4) the environmental field is statistically homogeneous and isotropic. While none of these assumptions is strictly valid for long-range propagation, the first three assumptions may be considered approximately valid in a perturbation sense. However, the inherent anisotropy and statistical inhomogeneity of the index of refraction in the vertical direction cause the fourth assumption to be extremely questionable.

Beran and McCoy[29-31] derived a solution in which the basic anisotropic nature of the two-point environmental statistic was retained together with the approximate form of the power spectrum of random temperature fluctuations in

the horizontal plane. One of the results of the Beran-McCoy formulation is given as follows

$$R_p(r,f,y,z) = I(z) \exp(-E_f f^{5/2} ry^{3/2}) = I(z) \exp(-E_k k^{5/2} ry^{3/2}) \qquad (55)$$

In this equation, the acoustic correlation function along a horizontal line transverse to the direction of propagation is an exponential function whose argument is proportional to E, an environmental parameter appropriate for the propagation path; the frequency f to the 5/2 power; the range R and the 3/2 power of Y the transverse separation distance of the two correlation points. The symbol I represents the intensity at a single point receiver with the same range and depth Z.

The components of the environmental parameter E for the finite source case are found by Beran and McCoy to be

$$E_f = 1.7(1/C_o \cdot \frac{\partial C_o}{\partial T})^2 A_T L_{\gamma m} (2\pi/C_o)^{5/2} \qquad * \qquad (56)$$

where $C_o$ is the nominal speed of sound, $\partial C_o/\partial T$ is the partial derivative of the sound speed with respect to the temperature, $A_T$ is the coefficient of the single term power-law spectrum representation of the random horizontal temperature variations (i.e., the nominal strength of the random temperature field), and $L_{\gamma m}$ is the correlation length of the random temperature fluctuations in the vertical direction. Thus the spatial coherence problem can be considered the experimental determination of the functional form of the coherence and the measurement of the coherence length. These specify the performance of the line array.

_____

*Note: If the expression for $R_p$ (eq. 55) is written in terms of wave number k instead of frequency f we have $E_f = (C/2\pi)^{-5/2} E_k$.

SPATIAL COHERENCE AND THE LINE ARRAY

Since the response of the array to the sound field is the convolution of the beam response of the array and the wavenumber spectra of the field, we can establish a resolution criteria by matching the angular spread in the incident field to the 3 dB width of the beam response. The spatial coherence function is a measure of this angular spread and can be evaluated as

$$S(k\sin\theta) = \int_{-\infty}^{\infty} R(y) \exp\{iks\sin\theta y\}dy \tag{57}$$

$$= \int_{-\infty}^{\infty} \exp(-(y/L_H)^n) \exp(iks\sin\theta y)dy$$

This integral can be evaluated in closed form for $n = 1, 2$ and numerically for $n = 1.5$. The results of this analysis when matched to the 3 dB width yield the following:

| n | BW (RAD) | BW (deg) | $L_a/L_H$ |
|---|---|---|---|
| 1 | $0.318 \; \lambda/L_H$ | $18.2° \; \lambda/L_H$ | 2.72 |
| 1.5 | 0.457 | 26.2° | 1.89 |
| 2.0 | 0.530 | 30.36° | 1.64 |
| $f_{\ell p}$ | 0.886 | 50.76° | 1 |

That is the exponential form has an angular spread of $0.318 \; \lambda/L_H$ and when matched with the 3 dB beam width of the line array $0.886 \; \lambda/L_a$ yields an aperture length 2.72 times the horizontal coherence length. Note that, given the same coherence length, the acoustic field angular spread for the Gaussian ($n = 2$) form is 1.67 times as large as the acoustic field angular spread for the exponential ($n = 1$) form.

In addition to matching the angular spread in the incident field to the beam width, one can compute the relative signal gain (RSG), that is, the ratio of actual signal gain to ideal signal gain. It can easily be shown that

$$RSG \simeq (L_H/L_a)^2 \int_{-L_a/L_H}^{L_a/L_H} (L_a/L_H - |x|) \exp(-x^n)dx \qquad (58)$$

This relationship shows that the relative gain of the system (when related to an exponential form of the spatial coherence function) is a function of the coherence length. Thus the angular resolution (beamwidth) and gain of the line array are determined by the coherence length and the form of the coherence function. This integral is calculated for and the results are shown in figure 7. The relative signal gain is plotted versus the length of the array in units of coherence lengths. The limiting value of $n = 1$, $1.5$, $2$ corresponding to the matched beam width ratio of $1.93$ for the Beran-McCoy form is also shown. The experimental determination of coherence length using the functional form shown in equation 55 allows one to bound the limits on array length due to the ocean volume.

EXPERIMENTAL RESULTS

To compare the theoretical correlation function with the acoustic measurements by Stickler[32], one must ascertain the value of the environmental parameter E that is appropriate for the experimental situation. The terms involved in the computation of E were obtained in the following manner. Because most of the acoustic data were based upon the transmission path[32] that intersected the array at approximately a 13° elevation angle, a ray tracing program was implemented to describe the path (range versus depth) of the 13° ray from the receiver, using measured sound speed profiles along a radial from the array at
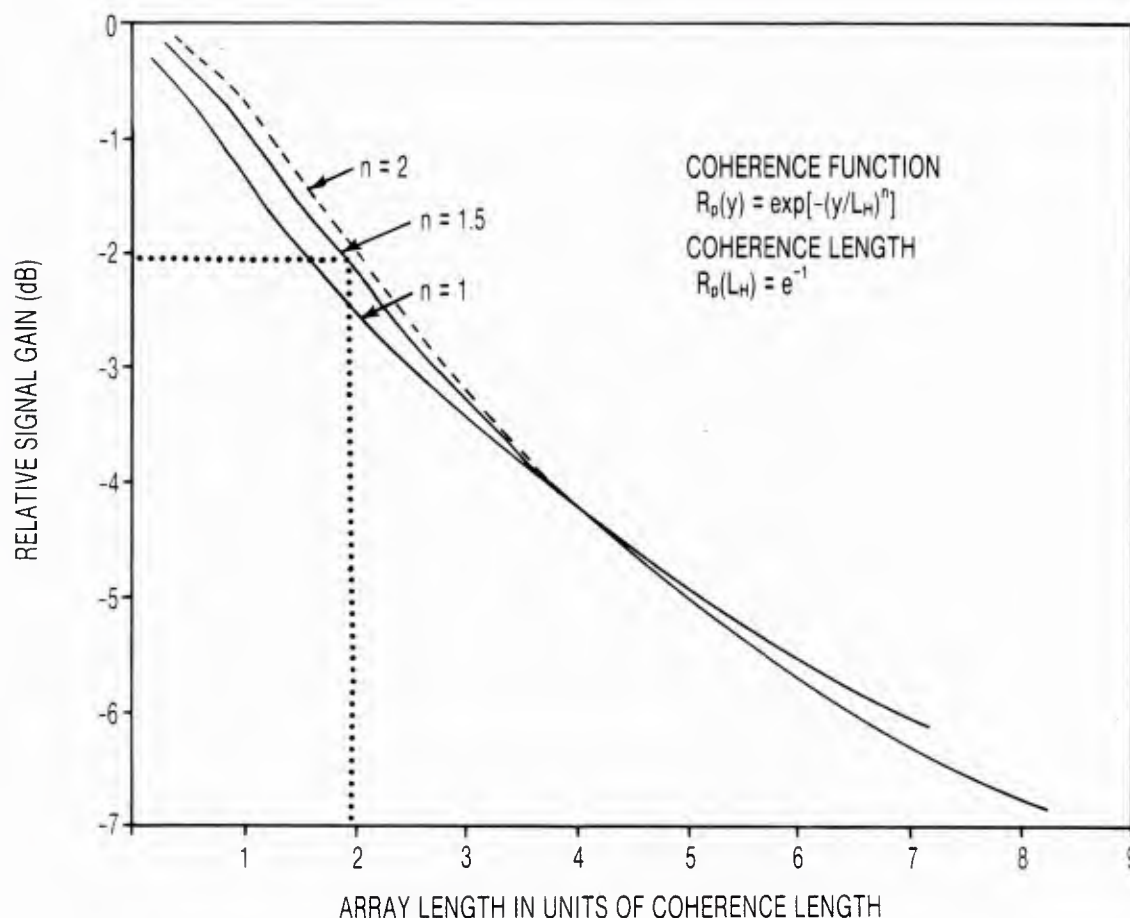
Figure 7.  Relative signal gain versus array length in units of coherence length for different coherence forms.

the azimuth of the experiment.  The average sound speed along the 13° ray path was 1517.5 m/s, and $c_o$ was set equal to this value.  The constant 3.6 m/s/°C was the value used for the partial derivative of the sound speed with respect to temperature, and this was obtained by evaluating the change with respect to temperature of Wilson's sound speed equation at a nominal temperature of 10°C.

The procedure that determined $A_T$ was as follows.  First, the Brunt-Väisälä frequency N was averaged along the 13° ray path, and the average value was found to be $1.5 \times 10^{-3}$ (rad/s).  Then the measured coefficients[33] to the single term power-law spectra for the random horizontal temperature fluctuations were treated as a function of N.  A linear extrapolation of the measured coefficient

from the nearest measured N to the average N along the 13° ray path indicates a value of $A_T$ of $1.5 \times 10^{-7}$ °$C^2$/m.

The normalized temperature spatial correlation function is equal to the inverse Fourier transform of the temperature spatial power spectrum normalized by the total variance; and the correlation length can be defined as the spatial length for which the value of the normalized correlation function is 0.5. Thus, the correlation length in the vertical direction of the temperature fluctuations was estimated by

$$0.5 = \int_a^b F_v(k) \cos(ks)\ dk / \int_a^b F_v(k)\ dk \qquad (59)$$

where $F_v$ is the vertical spatial power spectrum of the temperature fluctuations, k is the vertical wavenumber, s is the estimate of $L_{\gamma m}$, and a = .0209 rad/m and b = 20.94 rad/m. Millard[34] has data taken southwest of Bermuda which for the wavenumber interval under consideration can be approximated by $F_v(\kappa) = c\kappa^d$, where d is between 2 and 2.5. The value for s is $\simeq$ 35 m in the case when d is 2, s is $\simeq$ 28 m when d is equal to 2.5. It might also be noted that the theory of Garrett and Munk[35] would predict d to be equal to 2.5. As a result of these considerations, $L_{\gamma m}$ was given the nominal value of 30 m. Insertion of the values of into equation 58 yields the environmental parameter value

$$E = 4.8 \times 10^{-17} \qquad (60)$$

This environmental parameter was also calculated for sound speed profiles from the Mediterranean, Pacific and the Arctic and are summarized as below:

| | Dm | E | $L_c$ |
|---|---|---|---|
| Atlantic | 4000 m | $4.88 \times 10^{-17}$ | 1634 m |
| Mediterranean | 2000 m | 4.88 | 1634 m |
| Pacific | 3700 m | 9.31 | 1042 m |
| Arctic | 1600 m | 13.06 | 793 m |

Dm is the maximum depth over which the parameter E was averaged. The smallest E were for the Atlantic and Mediterranean whereas the largest was for the Arctic. The variation in E is 2.7 with a coherence length variation of 2. That is, the coherence length does not change by orders of magnitude as would be indicated without averaging the environment along the propagation path.

To compare measured acoustic results with the theoretical form of the correlation function without having a variable parameter E involved in each comparison, it is necessary to obtain an acoustic data base wherein the propagation is along environmentally similar paths. In addition, because the Beran-McCoy theoretical solution is strictly applicable only to single path propagation, path-resolving experimental capability is required.

The work of Stickler and Broek using a planer receiver in combination with short (10-ms ping) acoustic signal structure provided the required path resolution.[32]

During the acoustic measurements, steering delays correcting for average wave front curvature were constant for each experimental sequence that had time durations varying from 8 to 24 hr. The steering delays compensating for source motion were allowed to vary linearly with time during each experimental data sequence.

The acoustic data resulting from the experiments were reported as the average of the cosine of the phase difference between pairs of receivers and are plotted versus receiver separation. A direct comparison between the acoustic correlation function and the average of the cosine of the phase differences was justifiable because data indicated that above 100 Hz the phase fluctuations account for the predominant portion of the change in the acoustic correlation

for single path transmission. It should be noted that although some of the references included data for vertical separation between receivers, only data for horizontal separation between receivers (and transverse to the propagation direction) are used in this paper.

The Stickler data are shown in figure 8 and figure 9 for the center frequency of 400 Hz and ranges of 137 km and 259 km. We observe that the spread in the measured coherence values increases as the separation between receivers increases. Note, the median value of coherence decreases as the separation increases; and for a fixed signal to noise ratio, small values of coherence are difficult to measure and can be corrupted by the noise. These effects are consistent with the analysis of Devilbiss et al.[36] and Carter.[37,38] The results can be interpreted as: the measurement of phase in a random additive noise background requires a high signal-to-noise ratio. Even at 6 dB the uncertainty in the phase may be governed by the properties of the additive noise. Theoretical analysis of the measurement of the coherence of a fluctuating signal in an additive random noise background also shows that the coherence is a function of signal to noise ratio, with large confidence bounds. The conclusion drawn is the estimation of signal phase and coherence properties in the presence of a noise field such as the ocean ambient noise field is difficult. This conclusion is underscored by the spread in the data obtained by Stickler. The smooth curves in figures 8 and 9 are the calculations performed using the environmental parameter E and the McCoy formulism. In figure 10, the theoretical curve is repeated and the curves for all three exponential forms for the coherence function are shown where the correlation length was determined from the estimated (1/e) value observed in the data. The calculation utilizing the estimated E value seems to bound the data nicely especially if one assumes the downward spread in the coherence measurements could be due to the additive noise.

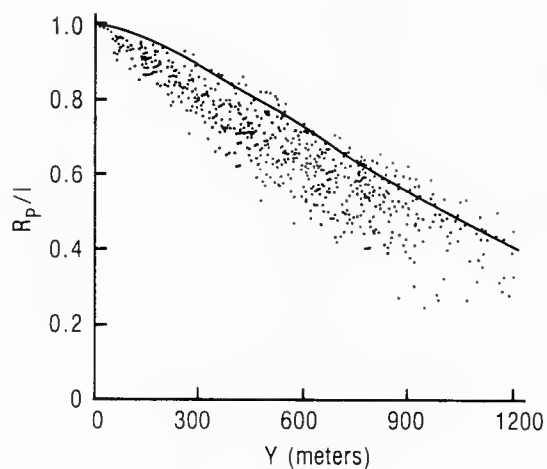Figure 8. Acoustic correlation versus transverse receiver separation: experiment three; range, 137 km; frequency, 400 Hz; curve represents theory.
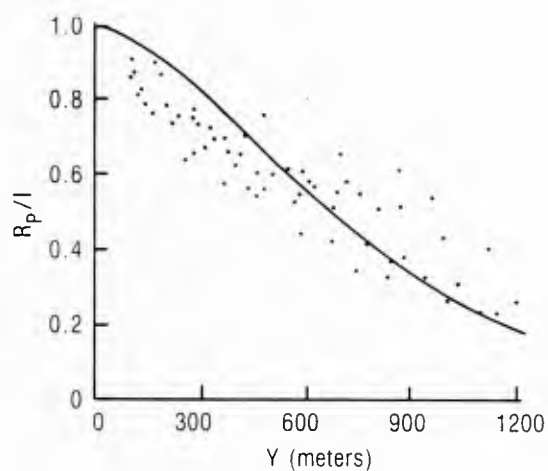
Figure 9. Acoustic correlation versus transverse receiver separation: experiment one; 259 km; frequency, 400 Hz; curve represents theory.
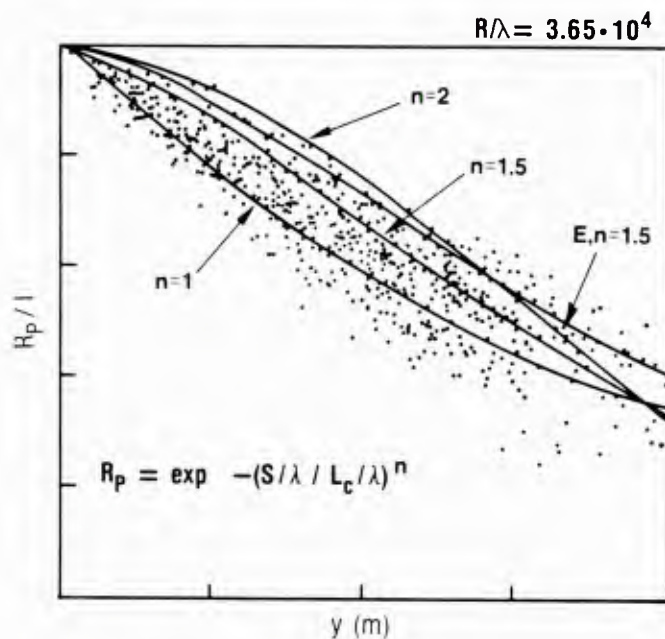


Figure 10. A comparison of $\exp(-(y/L_c)^n)$ with acoustic correlation versus transverse separation at 400 Hz.

Further, using the empirical estimate of coherence length, the n = 3/2 form provided a nice match to the data bounded on the upward side by the n = 2 form and the lower side by the n = 1 form.

Based on this comparison, we show in figures 11 and 12 the comparison of the calculated coherence versus range and coherence length versus range at 400 Hz based on the measurements of Stickler and Broek.[32] Note that the coherence lengths here are between 350 to 1647 m compared to the value of 3.4 to 6.4 km used by Dashen.[24] Ross Williams[39] has estimated coherence lengths at various ranges by visually smoothing phase time histories. His estimates ranged between 331 m and 1200 m at 400 Hz for ranges between 172 and 496 km as shown by the circles in figure 11. Finally, Kennedy[41] estimates the phase coherence length to be 183 m at 800 Hz and a range of 46 km. The Williams values are seen to be comparable to the Stickler-Broek values. Using the functional dependence on frequency to 5/2 power and range, we estimate that the Kennedy results would correspond to a length of approximately 353 m, the lower end of our range. Nevertheless, the spread in the data stresses our conclusion that the pairwise coherence is difficult to measure and is strongly influenced by the signal-to-noise ratio.
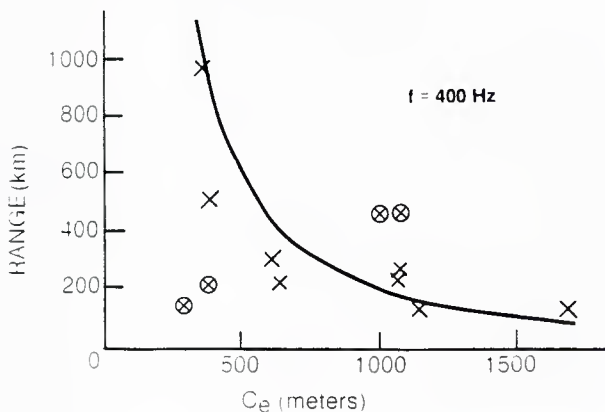


Fig. 11.  Acoustic correlation versus range; fixed receiver separation, 610 m; frequency, 400 Hz.
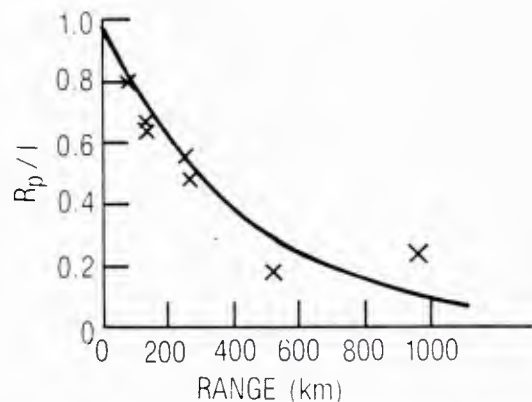
Fig. 12.  C versus range:  frequency, 400 Hz; curve represents theory.

To underscore this conclusion, magnitude squared coherence data is presented in figure 13 for two frequencies, 175 Hz from a moored source and 173 Hz from a towed source. The MSC curve for the 173 Hz tone shows a pronounced multipath interference pattern comparable to the signal-to-noise (S/N) variation. The results for the 175 Hz tone at high S/N (> 10 dB) replicates the S/N variations with increasing separations. These measurements were performed with a streamer behind a tow ship. Hence, as one approaches the ship, the interfering tow-ship radiated noise increases, the S/N decreases (< 10 dB), and the MSC shows wide variations due to the increase in the percentage of interfering noise. This result underscores the conclusions drawn that pairwise coherence is difficult to measure, is strong function of signal-to-noise ratio, and its bounds are large. The estimation of coherence must also be performed in a time that is short compared to the dynamics of the media and source-receiver motions. This is especially true when measurements are performed with a moving array.

## WAVENUMBER MEASUREMENTS

The signal coherence can be inferred from the measurement of coherent gain realized by the summation of n hydrophones at a given spatial wavenumber k

$$S_p(\omega,k) = \sum_{n=1}^{N} x_{np}(\omega) \cdot A_n \exp(i\phi_n(k)) \tag{61}$$

where $A_n$ is the array amplitude shading coefficient and $\phi_n(k)$ is a phase correction to steer the array in the k direction. An example of the beam output $|S_p(\omega,k)|^2$ is shown in figure 14. In figure 14a, one clearly sees the separation of signal energy and tow-ship noise and in figure 14b the beam response of the high signal level 173 Hz tone. The estimation of received coherent signal
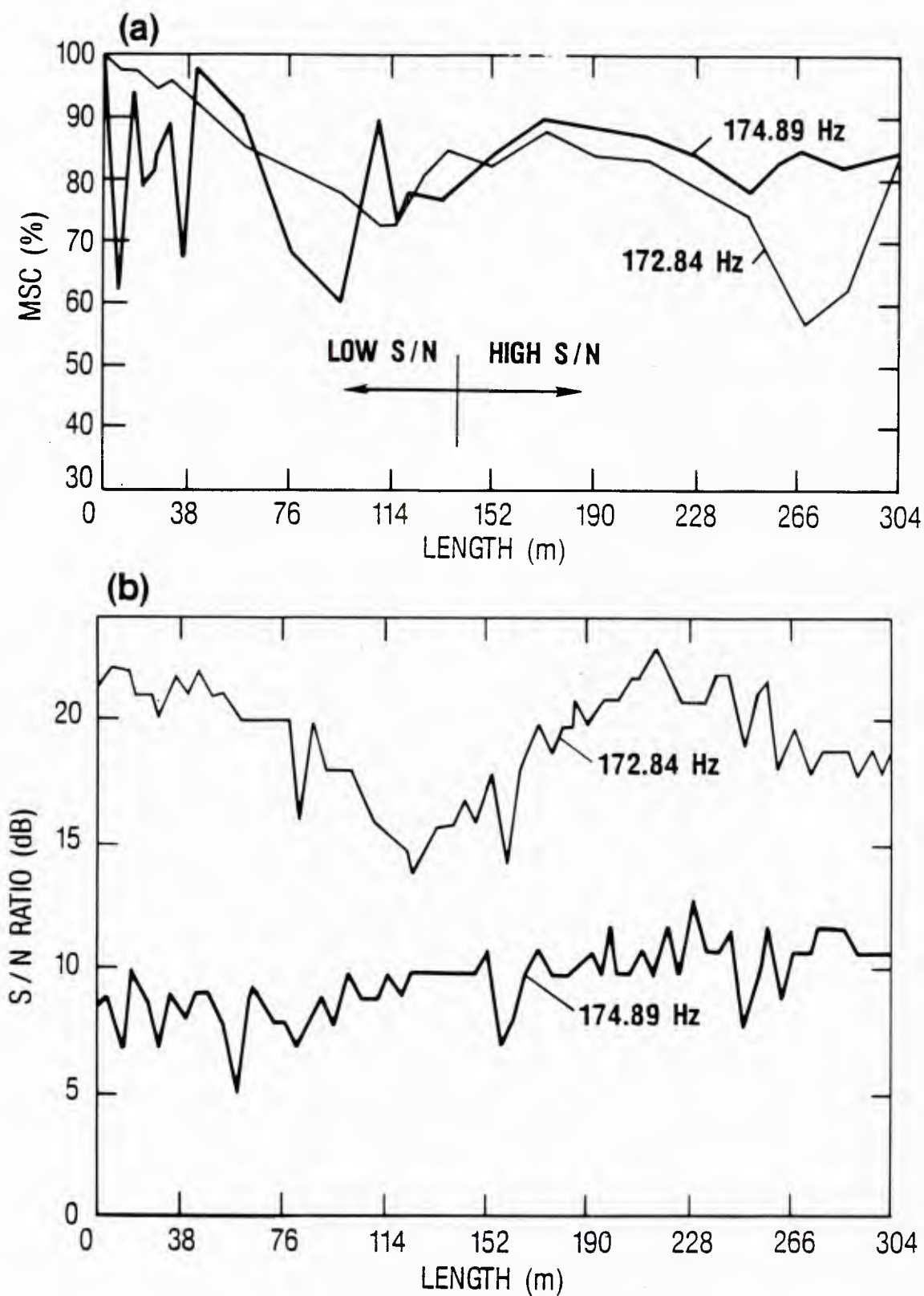
Figure 13.  Magnitude squared coherence (a) signal-to-noise ratio
(b) versus length along the streamer.

energy is easily performed at these beam signal-to-noise ratios. In this exam-
ple, the averaging interval used was too long when one considers the source-
receiver motion. Nevertheless, the peak signal-levels provided a good measure
of gain if the mean hydrophone level is known and a functional form of the
coherence versus transverse distance can be hypothesized. That is to say, the
difference between 20 Log (N) and the measured gain referred to as the relative
array signal gain (RASG) or the differential array signal gain (DASG) is deter-
mined by the degree of signal phase variability and consequently the degree of
coherence. The measurement uncertainties are reduced due to the large beam
signal-to-noise ratios and the increased number of degrees of freedom.

However, note in figure 14b the effect of beam broadening due to the mul-
tipath spread of off broad side arrivals is observed. Whereas this wavenumber
(angle domain) measurement of spatial coherence has the advantage of increasing
signal-to-noise ratio it is also susceptible to multipath and array deformation
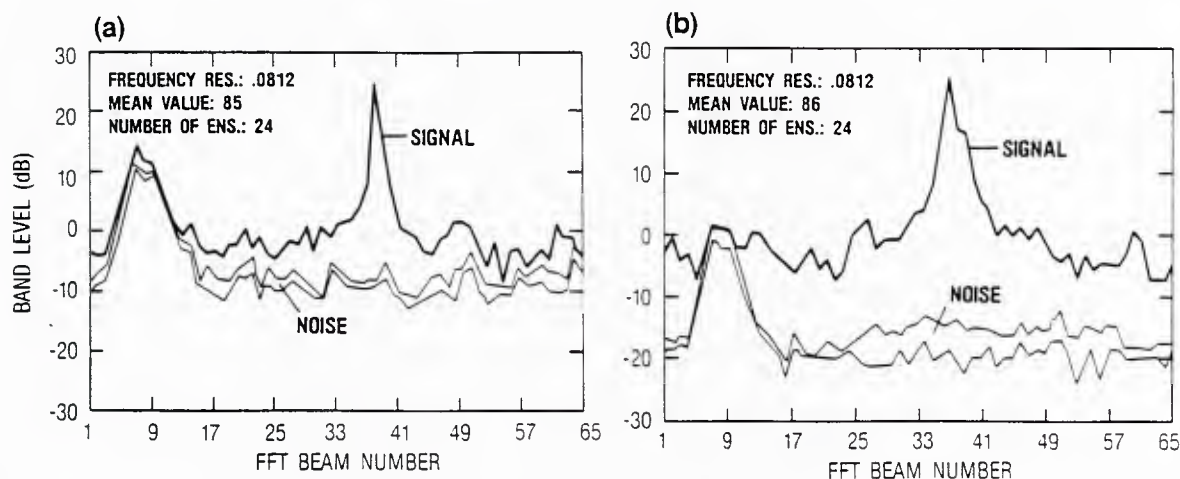effects.



Figure 14. FFT beam response versus wavenumber (FFT beam number) for the
signals from the 175 Hz moored source (a) and the 173 Hz towed
source.

Angle domain measurements made by W.B. Moseley (NRL)[42,43] with a line array of hydrophones positioned well within the sound channel in deep water are shown in figures 15 and 16. Figure 15a shows the average measured signal angular pattern (denoted by the solid curve) and the reference response (denoted by the thin curve) which would result from a completely coherent plan wave impinging upon a completely straight array. As indicated in the figure, there are several major differences between the measured and reference patterns. The array signal gain (indicated by the measured value at zero degrees) is degraded by about six dB relative to the ideal reference value while the three dB angular width of the measured signal is about twice as wide as that of the reference pattern. The measured distribution exhibits broad secondary maxima at angles different from the source direction (these will be shown to be due to multipath interference). Generally, the signal energy is distributed across angles instead of being restricted to a narrow main lobe with low side lobe structure as in the reference case. The causes of this increased spreading in angle are threefold--acoustic multipath interference, array deformations, and acoustic scattering due to random sound speed variations in the ocean. The effects of each of these mechanisms were examined individually and the results compared with the measured signal angular pattern to determine their relative influence.

Horizontal array deformations were independently measured during the experiment, and the lateral hydrophone displacements were used in computing deformed array beam patterns. Figure 15b gives the comparison between the average measured signal angular pattern and the computed average beam pattern for the deformed array (the thin curve). It is evident in the figure that the deformations of the array have contributed significantly to the loss in array signal gain and to both the observed spread of energy in angle and the increase
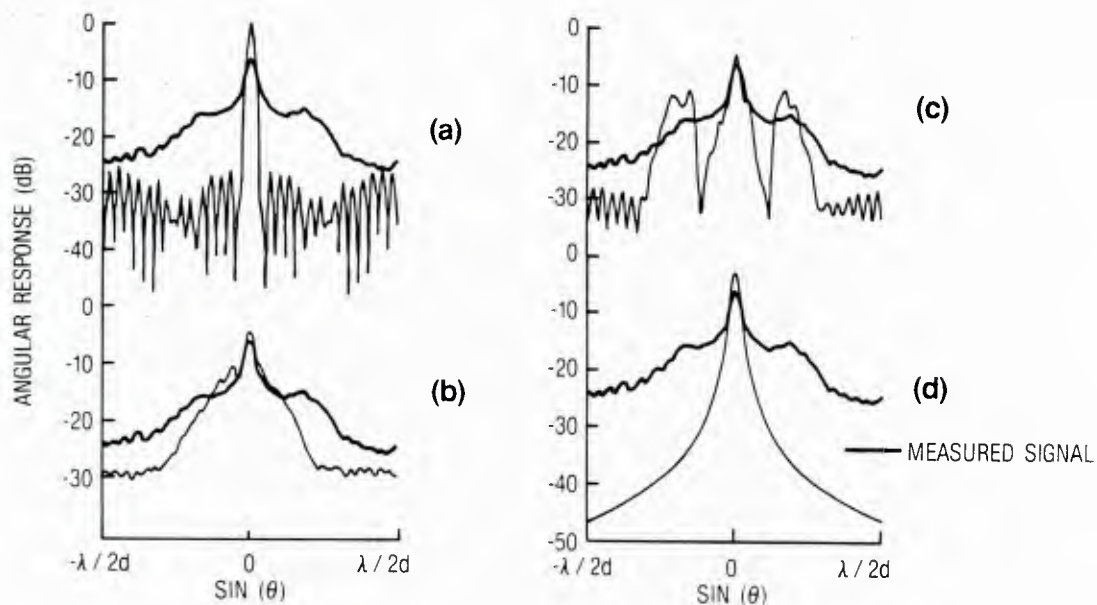
Figure 15. The average-measured beam response (dB) versus sinθ compared to computed beam response for (a) the case of an ideal array, (b) the case of a deformed array, (c) multipath interference, and (d) azimuthal scattering.
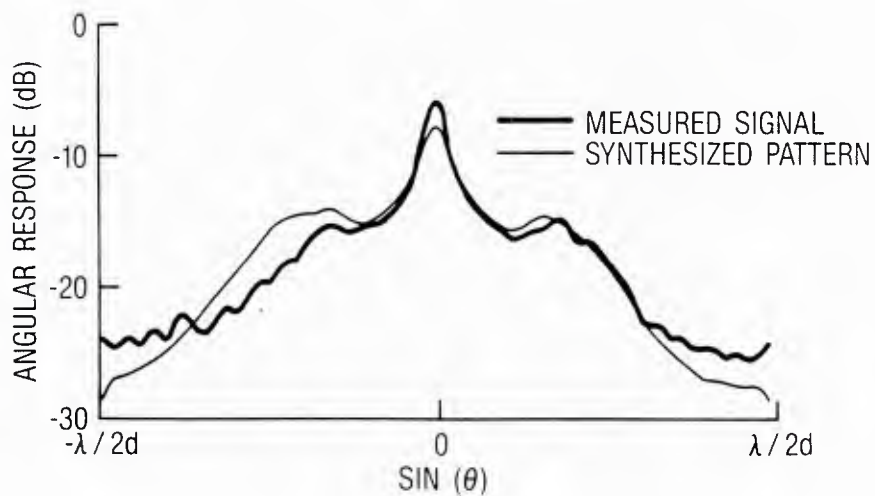


Figure 16. Comparison of measured and calculated beam angular response versus sinθ between ±λ/2d

in the three dB width. However, this mechanism does not account fully for any of these aspects of the measured signal distribution nor does it produce the broad secondary maximum ("shoulders") of the measured pattern.

The corrected parabolic equation propagation model[44,45,46] using as input the measured sound speed profiles between source and receiver was used to calculate the complex pressure field at the location of the receiver. Then standard beamforming was employed for a straight, predominantly horizontal but slightly tilted array (tilt was determined from independent hydrophone depth measurements) to determine its angular response in the presence of multipath interference. Figure 15c shows the angular array output due to multipath interference (the thin curve) in comparison with the average measured signal angular pattern. The comparison indicates that a substantial portion of the signal gain degradation is due to multipath interference, that this receiver has resolved part of the upcoming and downcoming energy, and that this energy would appear at the angles required to explain the broad secondary maxima or "shoulders" on the measured signal angular response.

The prediction of azimuthal scattering effects results from applying a space-angle Fourier transform to a spatial coherence function generated with the Beran and McCoy[29-30] treatment of propagation in a highly anisotropic random medium like the ocean, with the environmental factors computed from independent oceanic measurements. Figure 15d shows the theoretical azimuthal scattering effects (the thin curve) in comparison with the average measured signal angular pattern. As is shown in the figure, random medium scattering contributes only a small part to the degradation in array signal gain and the spreading of energy in angle. Here, its primary function is an angular smoothing influence on the effects due to array deformation and multipath interference.

As was suggested earlier, one must look to a combination of these mechanisms to predict the measured angular response. The predicted pattern shown in figure 16 was synthesized in the following fashion: with the incorporation of appropriate phase delays to simulate the measured horizontal array deformations, beamformer outputs were computed for the predominantly horizontal but tilted array located in the complex pressure field given for the presence of multipath interference by the corrected parabolic equation model; then this angular output was convolved with the theoretical azimuthal scattering pattern to arrive at the predicted pattern. Figure 16 gives the comparison between the predicted angular pattern (thin curve) and the average measured signal angular pattern (solid curve). There is now an agreement between the predicted and measured patterns to within 2.5 dB throughout almost all of the angular domain. Thus, the combination of multipath interference, array deformations, and acoustic scattering accounts for the array signal gain degradation, the change in three dB angular width, the "shoulders" in the measured pattern, and the general redistribution of energy in the angle domain.

TEMPORAL COHERENCE--FREQUENCY DOMAIN RESULTS[47]

Thus far we have discussed primarily the spatial coherence problem. Consider next, partial temporal coherence and spreading in the frequency domain. There have been a number of mechanisms investigated as causes of temporal coherence degradation including: small scale turbulence and mixing, surface scattering, mesoscale features like eddys, internal waves, and relative source-receiver motion. Small scale turbulence and mixing may be very important for the high frequency, short range problem; however, below 1000 Hz and for long range situations, these effects do not appear to strongly influence the results. Surface scattering produces acoustic sidebands shifted about 80-100

millihertz from the center frequency. On long time scales of days to months, mesoscale features (like eddys or rings) through their generation, motion, or decay can cause temporal changes in the received acoustic field. Yet these features by themselves are not critical to the coherent temporal signal processor design which is most concerned with variations of time scales from tens of seconds to tens of minutes. For low frequency, long range, and short time scales, the temporal coherence of the received field is dominated by two mechanisms. One is the internal wave (gravity waves within the ocean) modulation of the acoustic path structure. The other is a variation of the deterministic multipath interference pattern at the receiver caused by relative source-receiver motion.

Two examples of temporal variations causing spreading in the frequency domain are for the fixed source-fixed receiver case where ocean medium interactions with the propagating acoustic field dominate the results. Measurements for spreading in the frequency domain of an initially CW signal at 406 Hz transmitted from Eleuthera to Bermuda were obtained by Clark and Kronegold.[48] The spectral analysis of the phase and amplitude temporal fluctuations of the received signal showed substantial energy had been spread out to frequencies about 3 millihertz shifted from the carrier. A processor with a bandwidth of order 3 millihertz would accept the signal energy that has been spread in frequency and yet filter out extraneous noise energy. Another Eleuthera to Bermuda experiment was reported by Stanford.[49] His spectra were similar to those of the MIMI data in that the slope of the phase spectra are comparable ($f^{-2}$) and in that substantial energy has been spread out to about 3 millihertz. For the Eleuthera to Bermuda propagation path, the highest occurring Brunt-Väisälä frequency is of order 3 millihertz. Since internal wave energy is not present above the highest Brunt-Väisälä frequency and since these spectra show that

most of the significant energy is contained within the 3 millihertz spread, this is strongly suggestive that the internal wave mechanism was the dominant cause of spectral spreading for the fixed source-fixed receiver case.

Porter and Spindel[50] compared calculations with measurements to demonstrate when source-receiver motions were dominant. Three cases were considered: a fixed source-receiver, a slowly drifting receiver, and a rapidly drifting receiver. The first case was obtained for a fixed source-receiver geometry. A weak scattering ray theory for internal wave interaction by Porter and Spindel predicts the phase rate spectra to be a constant for frequencies less than the Brunt-Väisälä frequency with a rapid fall-off above this frequency. The predictions of their theory were shown to be in reasonable agreement with the measurements. The second case was the results for a slowly drifting sonobuoy (a drift rate of 0.05 knots) and the third case was for a rapidly drifting ship suspended hydrophone (a drift rate of 0.27 knots). The data were compared with the phase rate spectra predictions made by Porter and Spindel using a theory developed by Dyson, Munk, and Zetler[51] which assumes that the spectral behavior is dominated by deep amplitude fades caused by changing random multipath interference. The change from poor to good agreement between the Dyson, Munk, and Zetler model and the data as the drift rate increases was attributed to the increasing dominance of the source-receiver motion induced multipath interference effects.

The precise magnitude of source-receiver motion required to dominate a particular temporal spectrum has yet to be completely specified. Dashen, Flatte, Munk, and Zachariasen[52] have estimated that radial source motion of 0.33 knots and lateral motion of 2.2 knots will significantly influence the spectra. Dyer[53] has estimated that source-receiver motions of 3 to 5 knots

will produce dominance by multipath interference effects. Results of a treat-
mend of source-receiver motion induced deterministic multipath effects by
Clark, Flanagan, and Weinberg[54] shows a spread in the frequency domain of about
3 millihertz occurs for speeds of 5 knots. This implies that at 5 knots varia-
tions due to source motion may be comparable with those caused by internal wave
effects (assuming) that the source and receiver depths and sound speed profile
are appropriate). As the speed increases, the frequency spreading increases so
that for high rates of source motion a very narrow bandwidth processor would
filter out some of the source energy. Thus, both internal waves and source-
receiver motion can limit the useful frequency resolution of the processor.

In summary, the topics of acoustic spatial coherence and acoustic temporal
coherence have been treated in a conceptually simple but analogous fashion to
indicate that they are concerned with the spreading of the acoustic energy in
angle and frequency, respectively. For the long range, low frequency, short
time scale, predominantly refracted and refracted-surface-reflected energy
reception situation, the physical processes and environmental influences which
can degrade coherence have been indicated when the spatial and temporal effects
are separable. Three factors for the spatial case--acoustic multipath inter-
ference, array deformations, and scattering in a random medium--and two factors
for the single hydrophone temporal case--internal waves and source-receiver
relative motion--were shown to directly limit the resolution capability in
angle and frequency and thereby the receiving system gains. Over the past few
years theories and experiments have contributed to a better understanding of
the phenomena and have given verification in uncomplicated situations. How-
ever, usually the effects of the various factors are modeled separately. Theo-
ries need to be developed both for spatial and temporal coherence which treat
several factors simultaneously.

THE OBSERVATION OF MULTIPATHS

The propagation of mid-to-low frequency sound in the ocean to long range with refracted-refracted (RR) or refracted-surface-reflected (RSR) paths has been observed by several investigators (55,56) with arrays which separated the multipath arrivals. The separability of these arrivals by either a vertical or horizontal array is determined by the length of the array, its orientation, and the coherence length of the signal. The effective coherence length of the signal is determined, in this instance, by the amount of angular spread in the signal caused by diffused energy about a single arrival direction or by the distribution of energy in angle caused by the addition of several paths. Consider a plane wave from the $\theta_o, \phi_o$ direction with wavenumber vector $\underline{k}$ incident on an array along the x axis with a slight downward tilt $\psi$ as shown in figure 17.

$$\underline{k} \cdot \underline{x} / |\underline{k}| |x| = \cos\theta_a = \cos\theta_o \cos\phi_o \cos\psi + \sin\theta_o \sin\psi = \sin\theta_a' \qquad (62)$$
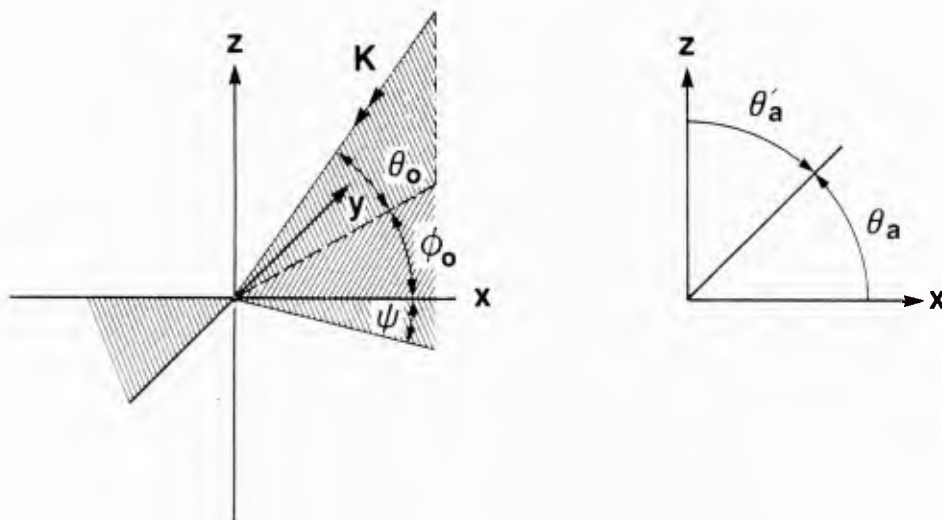


$$\cos\theta_a = \cos\phi_O \cos\theta_O \cos\psi + \sin\theta_O \sin\psi$$

Figure 17. The geometry.

We have shown from the off-broadside response of a uniform line array

$$2\Delta \sin\theta_a' = 2\Delta \cos\theta_a = 2\lambda/L \tag{63}$$

between the first nulls and for the half power (hp) points

$$(\Delta \sin\theta_a')_{hp} = (\Delta \cos\theta)_{hp} = 0.886\lambda/L \tag{64}$$

and at end-fire $(\Delta\theta)_{hp} = 2(0.886\lambda/L)^{1/2}$. For the off-broadside case, one can calculate a matched field condition where the angular spread of the signal is equal to the 3 dB beamwidth of the line array when the beam is steered in the direction of the signal.

$$L/(\lambda/\Delta \cos\theta_a) = L\cos\phi_o \cos\psi/(\lambda/\Delta \cos\theta_o) + L\sin\psi/(\lambda/\Delta \sin\theta_o) \tag{65}$$

The quantities $\lambda/\Delta \cos\theta_o = L_{eff}$, $\lambda/\Delta\cos\theta_o = L_x$, $\lambda/\Delta\sin\theta_o = L_z$ are interpreted as coherence lengths. When $L_x < L\cos\theta_o \cos\psi$, the horizontal component of the array over-resolves the field as the beam width for a given conical angle is narrower than the field. When $L\sin\psi > \lambda/\Delta\sin\theta_o$, the vertical resolution of the array due to its vertical extent over-resolves the field. When equation 65 is satisfied one has matched the field to the length of the system.

The angular spreads could be due to the distribution of energy about each path resulting from scattering, the different vertical arrival angles of independent paths, or the angular spread across the array due to a change in range.

The case of vertical arrival of different paths in the deep ocean can be estimated by use of Snell's law or Cox's ARAD[57,58] technique. Calculations with a representative Atlantic profile ($V_{os}$ = 1537 m/sec, $V_a$ = 1526 m/sec, $V_b$ = 1554 m/sec) and Snell's Law yield for the bottom grazing and surface grazing

rays $L_x$ = 90.9 $\lambda$ and $L_z$ = 14.4 $\lambda$. Using the ARAD technique with $\Delta\cos\theta \simeq V/V_o$, $\Delta/D^2$ = 0.17, and D(km) depth excess results in $L_x$ = 89 $\lambda/D$ and $L_z$ = 18 $\lambda/d$.

The deterministic multipath effects can be described by the methods of geometrical acoustics at the higher frequencies and by modes at the lower frequencies. The equivalence of modes and rays has been discussed by Guthrie and Tindle.[59] Here we use the ray-theoretic model, Trimain[60] and the normal model mode of Bucker[61] to illustrate these effects.

Figure 18a shows the path arrival structure as computed with the Trimain Code[60] at a frequency of 175 Hz for a source depth of 430 m and a receiver depth of 250 m. The ordinate is range in 0.2 km increments and the abcissa is the vertical arrival angle with 0° being the horizontal. At each range increment, the vertical line length represents the intensity for the eigenray at the angle corresponding to the intersection of the vertical line with the horizontal range line. Observe the angular difference and the convergence zone effects. The rate of change of arrival angle with range shows a definitive pattern with slopes between 0.44°/km to 0.16°/km. Shown in figure 18b is a similar case for the Ionian Basin of the Mediterranean. In this case the source is at a depth of 300 m, the receiver is at a depth of 250 m and the frequency is 175 Hz. This pattern is also distinctive with clear separable arrivals. The response of a slightly tilted horizontal array to the field is the convolution of the beam response pattern and the angular spectrum of the incident acoustic field. At any given range one can observe multiple arrivals the structure of which changes as the source-receiver separation is increased or decreased.
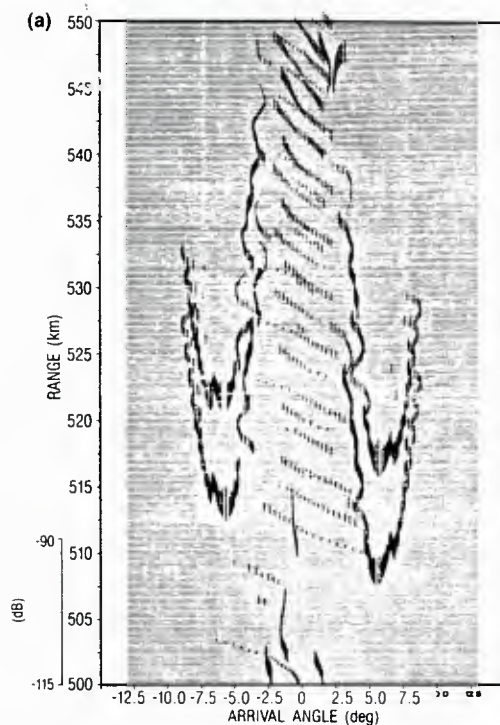
Fig. 18a. Computed eigen ray arrival
angle and intensity as a
function of range, Atlantic
Basin at 175 Hz.
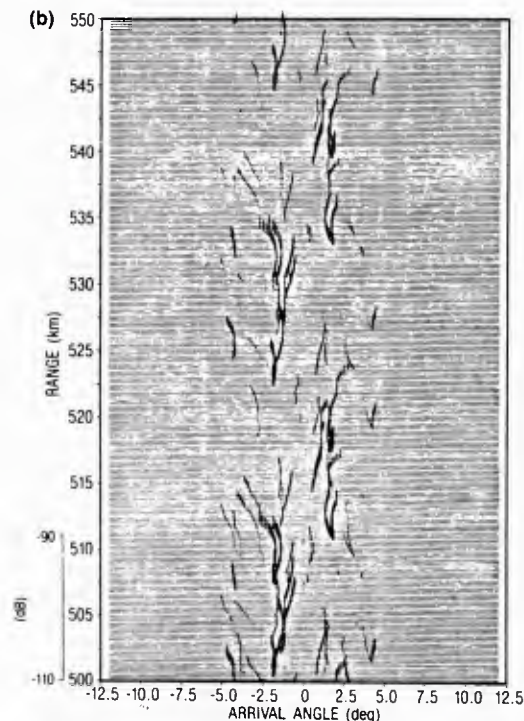
Fig. 18b. Computed eigen ray arrival
angle and intensity as a
function of range, Ionian
Basin at 175 Hz.

Figure 19 shows measured data obtained by Williams and Fisher[55] compared
to simulated data. The data are for the Pacific with a near surface source and
a receiver in the upper part of the sound channel in the mid-frequency range.
The arrival angles range between 8° and 14° in a clearly distinctive fashion
with a range rate of 0.143°/km. Thus the picture which data and calculation
show is one of multipaths at different angles which have definitive range rate
patterns. Similar results have been obtained by Lawrence and Ramsdale.[56]

These multipath patterns have been observed to change with time as the
properties of the intervening water column changes. These temporal effects
have been discussed in the preceeding sections. The question of the response
of an array moving in these fields is discussed later.

52

Figure 19. Measured and computed arrival angle versus range. (a) Measured arrival angles. (b) Calculated arrival angles versus range.

## SYNTHETIC APERTURE RESULT[62]

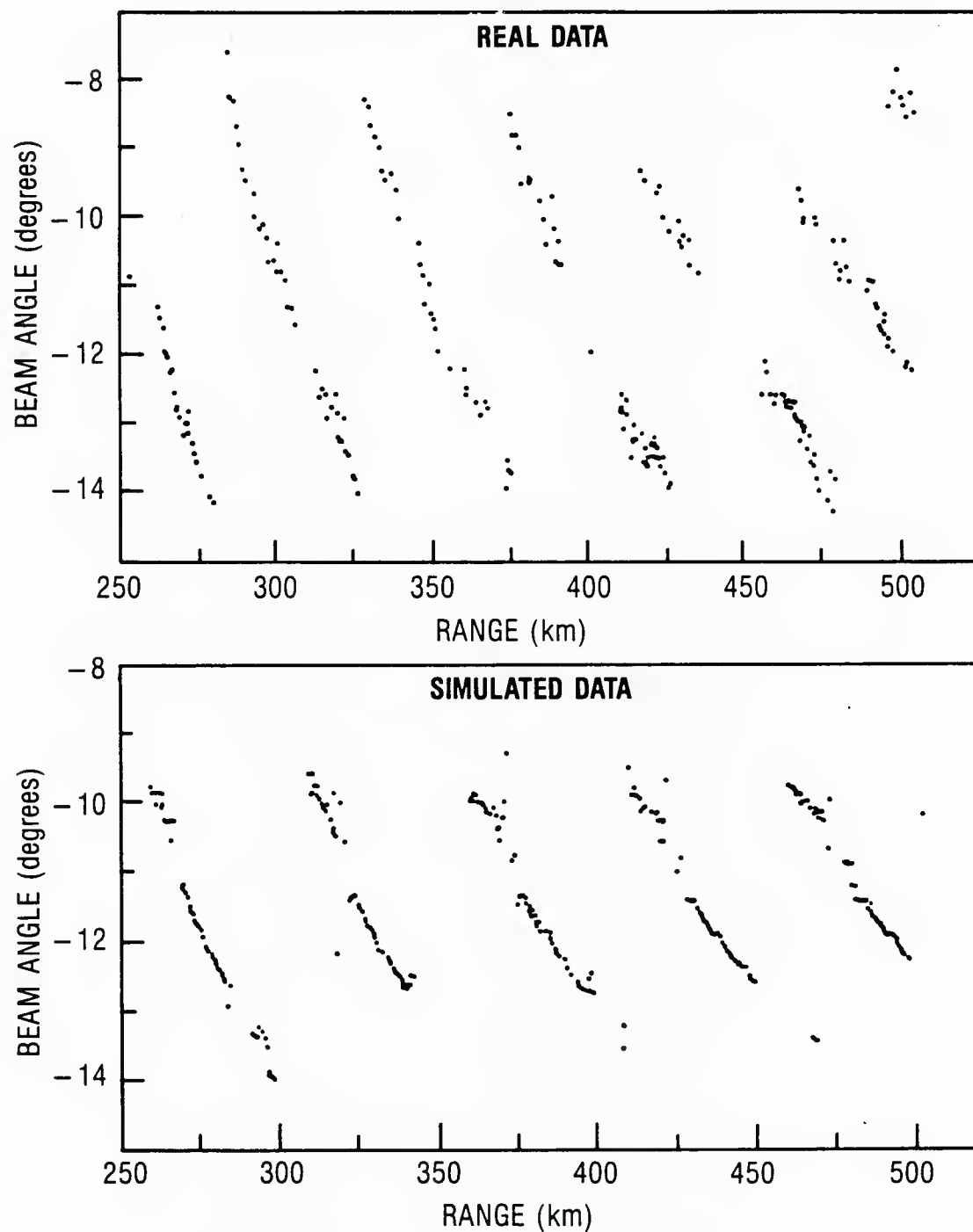Experimental results, shown in figure 20, demonstrate the formation of synthetic apertures when the source-receiver motion is known or inferred by a velocity filter, and when the synthetic aperture length is less than the signal coherence length, and when the processing time is less than the signal decorrelation time.

Synthetic apertures have been used in the field of radar since 1953. A monograph of classic papers in radar has been published by Kovaly.[63] Early attempts at the formation of synthetics in underwater acoustics concentrated on kHz frequencies and active systems. Sam Hanish (NRL) reviewed this field in 1975 and Louis J. Cutrona[64] published a paper in August of 1975 which discussed active sonar system design. In 1976, observations by Ross Williams[39] and R. Fitzgerald[40] based on single element phase records led to the speculation and conclusions that passive synthetic apertures could be formed. The Fitzgerald letter focused on a 10 Hz (150 m wavelength) signal over a distance of 65 km ($R/\lambda = 6.5 \times 10^3$) and the inference that apertures up to 3300 m ($L/\lambda = 22$) could be formed. This conclusion was not demonstrated by coherent summation of the signals or by the measurement of signal gain.

Ross Williams discussed phase versus time records obtained by a moored sensor and a moving source for distances up to 508 km ($R/\lambda = 10^4 - 10^5$) at a frequency of 400 Hz. He was able to find a linear trend between the average phase and time for several intervals during which he speculated that apertures up to 900 m ($240 \ L/\lambda$) could be formed. The effects of phase fluctuation and sensitivity of the technique to source-receiver motion were discussed by the author but were not incorporated into an estimate of coherent gain.
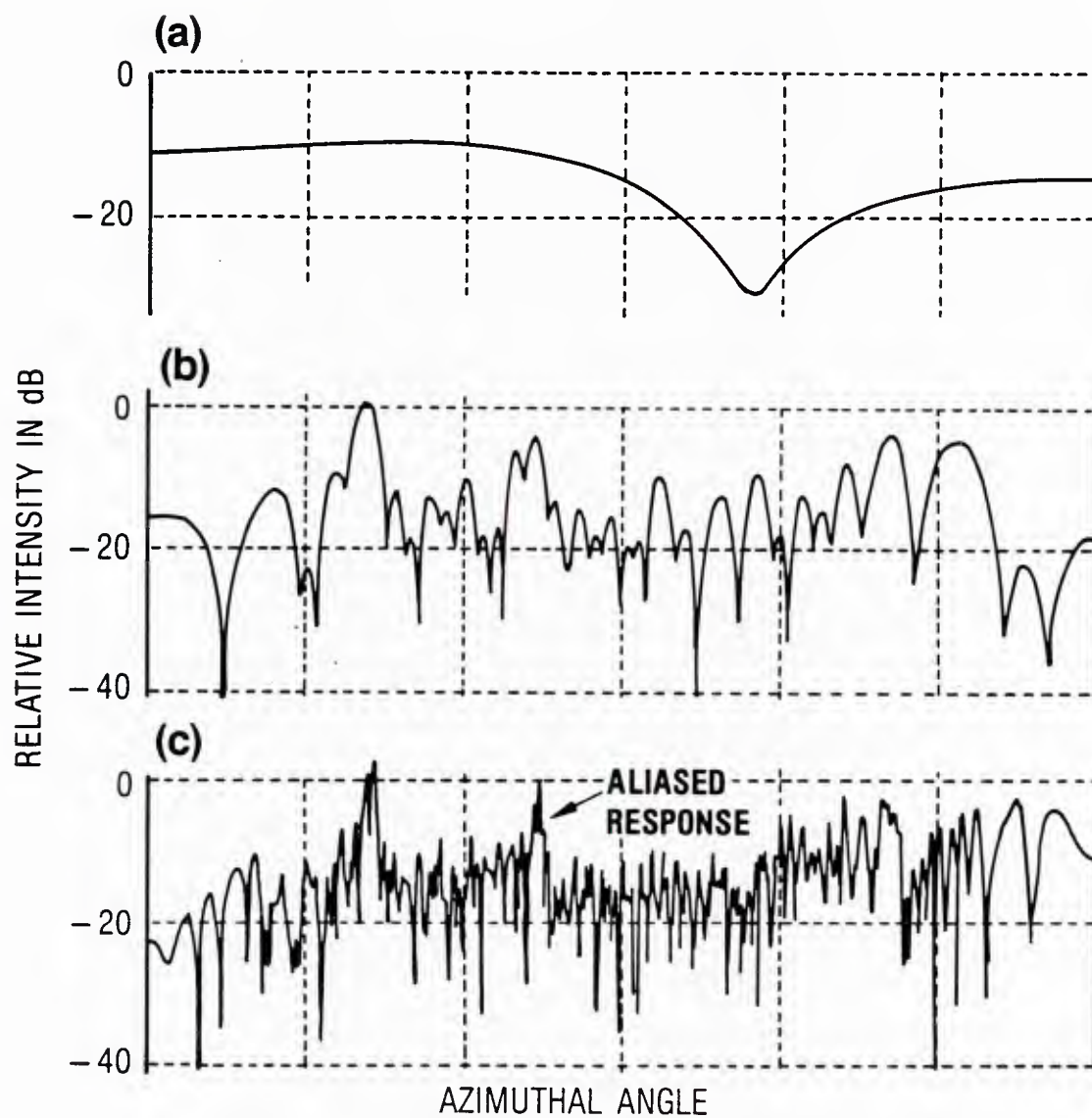
Figure 20.  Results of a synthetic aperture formed from sub-apertures with
four hydrophone groups.

Spindel and Porter[65] have also reported measurements at two frequencies (220-406 Hz) with drifting hydrophones over a source-receiver range of 260 km and showed during periods of highly correlated phase the formation of synthetic aperture length up to 8 km.

The data shown in figure 20 were obtained with four hydrophone groups spaced 0.3 $\lambda$ apart.[62] The response of the subaperture array was determined by

$$b(k_s,\theta_s,t_o) = \sum_{n=1}^{N} S_o \exp(i(\omega t_o - \underline{k}\cdot\underline{r}_n)) A_n \exp(ik\pi dn\cos\theta_s) \qquad (66)$$

$A_n$ represents the shading coefficient taken as unit and $\theta_s$ is the phase steering angle which determines the azimuthal response of the array. The formation of the synthetic aperture is accomplished by adjusting the successive beamformed outputs by a factor $\phi_m$ which should equal $\underline{k}\cdot\underline{V}m\Delta t$ in the direction of the arrival. The synthetic aperture result can be shown to be

$$B(k_s,t_o,t_o+n\Delta T) = [b(k_s,\theta_s,t_o)] \sum_{m=0}^{M=1} \exp(i(\omega m\Delta t - \underline{k}\cdot\underline{V}m\Delta t - \phi_m)) \qquad (67)$$

where $m\Delta t$ is the number of time intervals, $\underline{k}$ is the wavenumber vector and $\underline{v}$ is the source receiver velocity. The term $\omega m\Delta t$ accounts for the phase due to the time difference between $t_1$ and $t_{m+1}$. The term $\underline{k}\cdot\underline{V}m\Delta t$ accounts for the spatial distance $Vm\Delta t = \Delta L$ and the direction wavenumber vector $\underline{k}$.

The results shown in figure 20a show the response of the 1.2 $\lambda$ array, for which the arrival structure is not resolved. Second, figure 20b is the 23 $\lambda$ array which shows the direction of the source and an aliased side lobe due to the 2 $\lambda$ subaperture spacing. Figure 20c shows the 95 $\lambda$ array which begins to resolve the arrival structure. The aliased response is also evident. These

data show when the single path coherence length is greater than the length of the array and the temporal coherence length is greater than the processing time that synthetic apertures can be formed. The result shows the separation of arrival structure as the resolution of the array is increased. The off-broadside arrivals are seen to be affected by the vertical arrival structure. This result strongly implies that motion between the source receiver can also affect the beam response output.

DYNAMIC EFFECTS

The space-time measurement of the ocean acoustic pressure field has been described primarily for stationary sources and receivers. In these cases, the limiting resolution of the line array was shown to be due to the angular spread of the incident energy about a single arrival due to scattering phenomena or due to the addition of multipaths and their variation over the aperture. Previously, evidence obtained by Spindel and Porter as well as estimates by Dyer on the importance of multipath fluctuations and its dominance as relative motion between the source and receiver exceeds 1.5 m/sec was described. In these instances, the temporal and spatial resolution relationships are

$$\Delta f \cdot \Delta T \geq N \tag{68}$$

$$\Delta \theta_a \sin \theta_a (L/\lambda) = \Delta \theta_a' \cos \theta_a' (L/\lambda) \geq 1 \tag{69}$$

where

$$\sin \theta_a = \cos \theta_a' \text{ and } \cos \theta_a = \cos \phi_o \cos \theta_o \tag{70}$$

These relationships follow directly from our use of the Fourier transform and a rectangular sampling window. We observe that these relationships can become coupled by motion during the observation time.

$$\Delta\theta_{oa} = \frac{\partial\theta_{oa}}{\partial R}\,\Delta R + \frac{\partial\theta_{oa}}{\partial\phi}\,\Delta\phi = \frac{\sin\theta_o\,\cos\phi_o}{\sin\theta_a}\,\frac{\partial\theta_o}{\partial R}\,(L\cos\phi_o + V_R\Delta T)$$

$$+ \frac{\sin\theta_o\,\cos\theta_o}{\sin\theta_a}\,(V_\phi\Delta T/R) \tag{71}$$

This relationship can also be applied to the multipath problem as long as the angular separation between the paths is not great. We let $\Delta\theta_{oa}$ represent the angular spread due to the environmental factors and $\Delta\theta_a$ the beamwidth of the measurement system. When these two quantities are equal, we have matched the measurement system to the environment. When $\Delta\theta_a < \Delta\theta_{oa}$, we have the capability to resolve the multipaths and when the acoustic intensity is contained within a beam. A measurement problem of considerable interest is the resolution of distant shipping. In the following we will assume radial $(V_R)$ and azimuthal velocities $(V_\phi)$ of 10 m/sec, an azimuthal bearing of $\phi_o = 80°$, 90° being broadside, and measurement interval of 300 seconds.

By equating the aperture width with the angular spread, it can be shown that for a single path with a radial motion

$$\lambda/L = C_e g_o(\theta_o,\ \phi_o)\ (L\cos\phi_o + V_R\Delta T) \tag{72}$$

$$g_o(\theta_o,\ \phi_o) = \sin\theta_o\,\cos\phi_o,\ C_e = |\partial\theta_o/\partial R|$$

The constant $C_e$ is the rate of change of single path vertical arrival angle $(\theta_o)$ and can be taken from the previously shown vertical arrival angle plots. This constant is small $O(2\times10^{-6})$ and near convergent zones, $O(8\times10^{-5})$.

The azimuthal variation for the single path case can also be shown to be:

$$\lambda/L = \sin\phi_o\,\cos\theta_o\,V_\phi\Delta T/R \tag{73}$$

Where R is the radial distance to the source taken here to be 70 km. Similar results can be obtained for the multipath case and are given by

$$\lambda/L = \cos\phi \; \Delta\cos\theta \; \{1 + (\frac{1}{Wr_o}) \; |\frac{\partial\Delta\theta_o}{MR}| + g_1|\frac{\partial\theta_o}{MR}| \; V_R\Delta T\}$$

$$+ \frac{\cos\theta_o \; \sin\phi_o}{R} \; V_\phi\Delta T \qquad\qquad (74)$$

$$g_1 = \tan^2\phi_o \; / \; \tan\theta_{ol} \; (\tan^2\phi_o + \sin^2\theta_{ol})$$

The multipath case shows a constant term determined by the initial spread in angle between the paths, a radial term which accounts for the change in spread with range, a radial term which accounts for the variation in central arrival angle with range and finally a term which accounts for the azimuthal rate of change.

These results are interesting as they allow us to rank the relative importance of these effects on the ocean measurement problem. When motion is not important the single path refraction result yields

$$L/\lambda \rightarrow 8 \times 10^3/\sqrt{\lambda}$$

Comparison with results from the "Experimental Results" section indicates that in this instance the measurement will be dominated by volume or surface scattering. When the motions are extreme we find

$$L/\lambda \rightarrow (1/C_e) \; g_o \; V_R\Delta T \simeq 3 \cdot 10^4$$

and again scattering not refraction limits the ability to measure the single path arrival. These results confirm our previous discussion regarding single path propagation and volume scattering.

We can continue the process and estimate term by term the relative importance of each effect.  For the specific example given here, we have tabulated these results in the following table.

## A Comparison of Multipath/Motion Effects

| CASE | $L/\lambda$ | REMARKS |
|---|---|---|
| Single Path | | |
|     Static | $8 \times 10^3/\sqrt{\lambda}$ | $V_r = 0$    Scattering is dominant. |
|     Dynamic (radial) | $4 \times 10^3$ | $V_r > 20$ |
|     Dynamic (azimuthal) | 25 | at R = 70 km, azimuthal motion is very important |
| Multipath | | |
|     Static (Atlantic) | 525 | $\phi_o = 80°$ |
| | 105 | $\phi_o = 30°$ |
| | $506/D \simeq 84$ | Cox's ARAD, D(km) |
| Dynamic $V_r = V_\phi = 0$ | 302 | Here we use a case with $\theta_{01} = 8.5°$, $\theta_{02} = 16°$ |
|     $V_\phi = 0$, $V_r = 20$ | 278 | |
|     $V_\phi = 0$, $V_r = 20$ | 67.3 | CZ case |
|     $V_\phi = 20$, $V_r = 0$ | 21.6 | |

The results, although only given for a specific measurement problem, clearly show the importance multipath arrival structure and motion have on the resolution capabilities of the ocean measurement system.  Measurements performed with arrays to measure horizontal noise directionality should carefully consider these results.  We have used only horizontal arrays with no tilt or vertical extent.  These results can easily be extrapolated to the case of a tilted array and the procedure applied to the case of a vertical array.  The

results thus far have used the vertical arrival structure for the Atlantic, figure 18a. These results scale to the cases of the Pacific, figure 19, and the Mediterranean, figure 18b.

Figure 21 illustrates a numerical calculation using a normal mode model and a Mediterranean sea profile. The array has a slight tilt and the beam response and illumination function are plotted versus range. We observe the variation with range in the array illumination pattern due to the combinations of multipath and the subsequent bifurcation of the beam response. The results are plotted in 1 km intervals and provide a graphic illustration as to variation expected in range as a function of source receiver motion. The range change during a measurement period of 300 seconds is 154.2 m/knot. Since the variations with range are on the order of 1 km, we can expect dramatic variations as our speed approaches 3 knots. This result is wholly consistent with our previous comments regarding multipath fluctuations.

The conclusion drawn here is that the resolution of multipath arrivals with a horizontal array with slight tilt occurs well before single path limits are reached. Furthermore, relative motions of the source of sound, i.e., a surface ship, further impact the choice of measurement parameters available at a given frequency, that is, the array length, and the observation time. These results should apply to many ocean measurement problems such as the determination of the role of shipping on the directionality of noise.
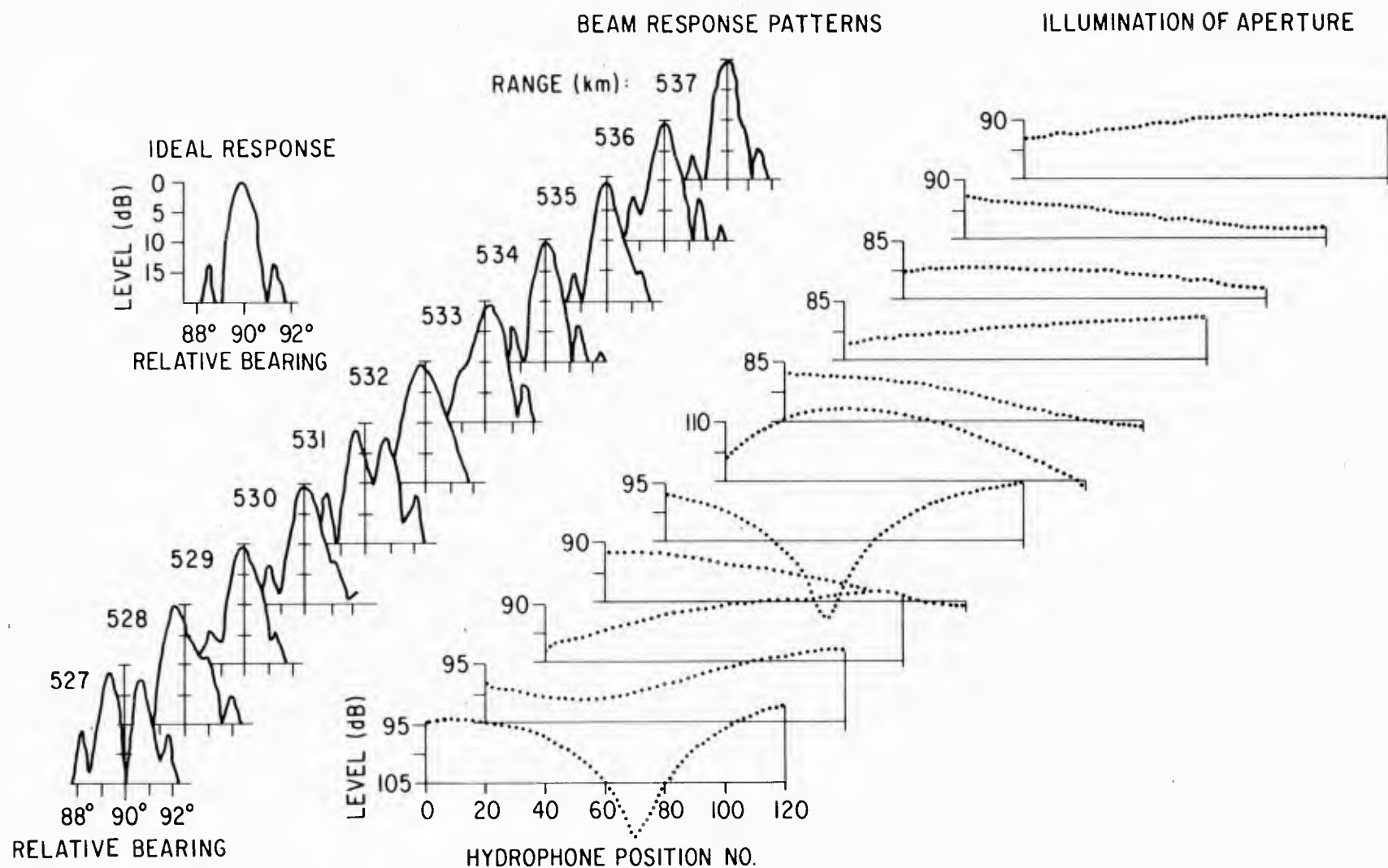
Figure 21.   Calculated near-broadside beam response patterns and illumination of aperture as a function of range.

## SUMMARY AND CONCLUSIONS

This paper had as its focus the problem of ocean-acoustic measurements with line arrays. The space-time transforms were reviewed to demonstrate the analogy between spatial and temporal properties, to stress the importance of convolution and matched field processing. A criteria was presented by which the resolution of such measurement systems could be calculated.

The static source-receiver case was shown to be influenced by the randomness in signal phase due to scattering and closely following the method and approach of Shifrin, we show the results of this Gaussian phase randomness and the importance of the coherence functional form. Calculations and data were employed to show the importance of multipath effects on the relative gain of line array measurements systems and the difficulties encountered for the determination of coherence lengths. Single path coherence lengths were found to be large and predictable using an environmental parameter E and the Beran-McCoy mutual coherence function of form. Nevertheless, multipath effects were in our opinion dominant.

The temporal fluctuation problem was briefly introduced for completeness but also to stress the finding that for relative source-receiver speeds of 1.5 m/sec (3 knots) or greater, the fluctuations are dominated by the changes in the multipath arrivals. These effects dominate most measurements. We illustrate slowly moving source-receiver and show with data that a line array can resolve distinct multipath arrivals. We presented a simplified analytical formulism for the determination of the aperture length required to contain the multipath arrival during the measurement period or for the determination of the length of the system required to resolve two distinct arrivals.

In closing, we conclude that vertical and horizontal line arrays are merely spatial transforms analogous to temporal transforms. The spatial structure, angular spread, determines the length of the antenna required either to characterize the structure or to contain the structure within a spatial wavenumber interval.

When the incident signal is a wave with a normal variable in phase, the net gain was shown to proceed according to a $2L/\lambda$ until the spread in incident energy becomes greater than the spatial beamwidth half power points, that is, a saturation effect. We conclude that this beginning of saturation is one limit on measurement system resolution.

When the vertical arrival angles from multiple paths project horizontal angles greater than the half-power beam widths, beam bifurcation occurs. For vertical arrays, we simply have the arrivals on different beams. Horizontal arrays have an azimuthal variation in the resolution from broadside to end fire. Our calculations and data result in the conclusion that the combined effect of antenna distortion and multipath arrival structure are exceedingly important in the ability of the system to measure the incident field.

Motion of the source-receiver with respect to one another couples the space-time processing problem. We concluded that for static cases we must restrict our processing to temporal and spatial coherence lengths determined by either the temporal or spatial correlation function. However, when the relative motion becomes important ($>1.5$ m/sec), we are restricted to an effective length determined by the time required to perform the measurement and the variation of the multipath arrival structure.

The measurement of the signal gain of a spatial array requires either the determination of the phase moments, the spatial coherence or the coherent output of the line array. Whereas it is difficult to measure signal phase or coherence at low signal-to-noise ratios and large separations, it is possible to measure the coherently summed output of the array. This sum can be related to the mutual coherence function and consequently the coherence length estimated. Thus, high resolution, large arrays may provide a tool by which spatial coherence lengths can be estimated in the low- to mid-frequency region.

In the case of the spatial coherence problem, a theory is required that combines and includes both the scattering and the multipath interference effects simultaneously. For the temporal coherence problem, a theory is needed that incorporates both the internal wave modulation of the acoustic path structure and the variation of the multipath interference pattern due to relative source-receiver motion. These are current areas of activity by several research groups. A complete theory which treats both temporal and spatial coherence simultaneously (including the several influential factors for each) is in all likelihood some years away from development. However, a precise predictive capability for either or both of the acoustic field coherence properties will influence both array and processor usage.

# REFERENCES

1. A.A. Winder, and C.J. Loda, Introduction to Acoustical Space-Time Information Processing, ONR Report ACR-63, Wash., D.C., 1963, Republished, Peninsula Publishing, P.O. Box 867, Los Angeles, CA 94022.

2. S.O. Rice, "Mathematical Analysis of Random Noise," Bell Sys. Tech. Journal, VOLS 23 and 24: Selected Papers on Noise and Stochastic Processes, pp. 133-294, Dover Publications, New York, 1954.

3. P. Middleton, An Introduction to Statistical Communication Theory, McGraw-Hill Book Co., New York, 1960.

4. Y.W. Lee, Statistical Theory of Communication, John Wiley and Sons, New York, 1960.

5. E.A. Robinson, Statistical Communication and Detection, with Special Reference to Digital Signal Processing of Radar and Seismic Signals, Hafner Pub. Co., New York, 1967.

6. R.C. Bourret, "Directivity of a Linear Array in a Random Transmission Medium," J. Acoust. Soc. Am., 33 (12), pp. 1793-1797, 1961.

7. H.G. Berman and A. Berman, "Effects of Correlated Phase Fluctuations on Array Performance," J. Acoust. Soc. Am., 34 (5), pp. 555-562, 1962.

8. D.J. Bordelon, "Effect of Correlated Phase Fluctuation on Array Performance," J. Acoust. Soc. Am., 34 (8), pp. 1147, 1962.

9. J.L. Brown, "Variation of Array Performance with Respect to Statistical Phase Fluctuation," J. Acoust. Soc. Am., 34 (12), pp. 1927-1928, 1962.

10. G.E. Lord and S.R. Murphy, "Reception Characteristics of a Linear Array in a Random Transmission Medium," J. Acoust. Soc. Am., 36 (5), pp. 850-854, 1964.

11. D.J. Bordelon, "Comments on 'Reception Characteristics of a Linear Array in a Random Transmission Medium,' by Lord and Murphy," J. Acoust. Soc. Am., 37 (2), pp. 387, 1964.

12. Yakov Solomonovich Shifrin, Statistical Antenna Theory (Published by Sovietskoye Radio, Moscow 1970). The Golem Press, 1971, Box 1342, Boulder, CO 80302. (Also Hanish, NRL - Private Communications.)

13. B.D. Steinberg, Principles of Aperture and Array System Design, John Wiley and Sons, New York, 1976.

14. F.J. Harris, "On the Use of Windows for Harmonic Analysis with Discrete Fourier Transform," Proc. IEEE, 66 (1), pp. 51-83, Jan. 1978.

15. S.L. Marple, Jr., and S.M. Kay, "Spectrum Analysis," Proc. IEEE, 69 (11), pp. 1380-1418, Nov. 1981.

16. W.C. Knight, R.Q. Pridham, and S.M. Kay, "Digital Signal Processing for Sonar," Proc. IEEE, 69 (11), pp.1451-1506, Nov. 1981.

17. R.A. Wagstaff and A.B. Baggeroer, "High-Resolution Spatial Processing in Underwater Acoustics," NORDA, MS., 1983.

18. The use of the factor $(1/2\pi)^4$ in equation 3 can be changed by using $(1/2\pi)^2$ in the definition of both the transform and its inverse or by a change in the variables $\omega$ and k to f and $k/(2\pi)^3$.

19. Lord Rayleigh, Phil; Mag 43, p. 259, 1897.

20. L.A. Chernov, Wave Propagation in a Random Medium, Moscow, 1958; English Translation: McGraw-Hill, New York, 1960.

21. U.I. Tatarski, Wave Propagation in a Turbulent Medium, McGraw-Hill, New York, 1961.

22. S.M. Flatte, R. Dashen, W.H. Munk, K.M. Watson, and F. Zachariasen, Sound Transmission through a Fluctuating Ocean, Cambridge Univ. Press, New York, 1979.

23. S.M. Flatte, "Wave Propagation through Random Media: Contributions from Ocean Acoustics," Proc. IEEE, 71 (11), pp. 1267-1299, Nov. 1983.

24. R.F. Dashen, S.M. Flatte, W.H. Munk, and F. Zachariasen, "Limits on Coherent Processing due to Internal Waves," Standford Research TR-JSR-76-14 (Avail DTIC), Standford Research Inst., Menlo Park, CA.

25. Yves Desaubies, "Statistical Aspects of Sound Propagation in the Ocean," Adaptive Methods in Underwater Acoustics, edited by H. Urban, D. Reidel Pub. Co., Boston, MA.

26. J. McCoy, "Propagation of Spatial Coherence in the Deep Ocean: A Theoretical Framework," Stochastic Modeling Workshop, Oct. 26-28, 1982, ARL/ Univ. of Texas at Austin, Austin, TX 78712, 1983.

27. K.M. Guthrie, "The Persistence of Acoustic Multipaths in the Presence of Ocean Volume Scattering," Stochastic Modeling Workshop, Oct. 26-28, 1982, ARL/Univ. of Texas at Austin, Austin, TX 78712, 1983.

28. H. Cox, "Line Array Performance when the Signal Coherence is Spatially Dependent," J. Acoust. Soc. Am., 5416, pp. 1743-1746, 1973.

29. M.J. Beran and J.J. McCoy, "Propagation through an Anisotropic Random Medium," J. Math. Phys., 15 (11), 1901, 1974. Also ref: Beran, M.J., and McCoy, J.J., "Propagation of Radiation from a Finite Beam or Source through an Anisotropic Random Medium," J. Acoust. Soc. Am., 56 (6), 1667, 1974.

30. M.J. Beran, J.J. McCoy, and B.B. Adams, "Effects of a Fluctuating Temperature Field on the Spatial Coherence of Acoustic Signals," NRL Report 7809 (1975).

31. U. Frisch, Probabilistic Methods in Applied Mathematics, Academic Pressing, New York, 1968.

32. D.C. Stickler, R.D. Worley, and S.S. Jaskot, Bell Laboratories Unpublished--Summarized by Robertson, G.H., "Model for Spatial Variability Effects on Single-Path Reception of Underwater Sound at Long Ranges," J. Acoust. Soc. Am., 69 (1), pp. 112-123, 1981.

33. W.B. Moseley, D.R. DelBalzo, "Oceanic Horizontal Random Temp. Structure," NRL Report 7673, 1974.

34. R. Millard, Private Communication.

35. G.V. Garrett, W. Munk, "Space-Time Scales of Internal Waves, A Progress Report," J. Geophysics Re 80 (3), 271, 1975.

36. G.E. Devilbiss, R.L. Martin, and N. Yen, "Coherence of Harmonically Related CW Signals," NUSC-TA11-C22-74, Availabe DTIC, 1981.

37. G.C. Carter, C.H. Knapp, and A.H. Nuttall, "Statistics of the Esimate of Magnitude-Coherence Function," IEEE Transactions on Audio and Electroacoustics, AU-21 (8), pp. 388-389, 1973.

38. E.H. Scannell, C.Q. Carter, "Confidence Bounds for Magnitude-Squared Coherence Esimates," Proc. IEEE International Conference on Acoustics, Speech and Signal Processing, pp. 670-673, 1978. Also see Carter, C.G., Scannell, E.H., NUSC T.D. 5881, 1978.

39. R.E. Williams, "Creating an Acoustic Synthetic Aperture in the Ocean," J. Acoust. Soc. Am., 60 (1), pp. 60-72, 1976.

40. R.M. Fitzgerald, A.N. Guthrie, and J.D. Shaffer, "Low-Frequency Coherence Transverse to the Direction of Propagation," J. Acoust. Soc. Am., 60 (3), pp. 732-753, 1976.

41. R.M. Kennedy, "Phase and Amplitude Fluctuations in Propagating through a Layered Ocean," J. Acoust. Soc., Am., 46 (3P2), pp. 737-745, 1969.

42. W.B. Moseley, "Acoustic Coherence in Space and Time--An Overview," EASTCON 78.

43. W.B. Moseley, "Geographic Variability of Spatial Signal Correlation and Subsequent Array Performance," International Symposium on Underwater Acoustics, Telaviv, Israel, June 15-18, 1981.

44. J.A. DeSanto, "Relation between the Solutions of the Helmholtz and Parabolic Equations for Sound Propagation," J. Acoust. Soc. Am., 62, 295-297, 1977.

45. J.A. DeSanto, J.S. Perkins, and R.N. Baer, "Corrections to the Parabolic Equation for Sound Propagation Modeling," Private Communications.

46. J.S. Perkins and R.N. Baer, "A Corrected Parabolic-Equation Program Package for Acoustic Propagation," NRL Memorandum Report 3688 (1978).

47. R.P. Porter, "SOFAR Propagation of Wide-Band Signals to Long Ranges," International Workshop cn Low Frequency Propagation and Noise, Woodshole, MA, 14-19 Oct. 1974, Vol. II (V), p. 633, Maury Center for Ocean Science, Wash., D.C., 1977.

48. J.G. Clark and M. Kronengold, "Long-Period Fluctuations of CW Signals in Deep and Shallow Water," J. Acoust. Soc. Am., 56, pp. 1071, 1974.

49. G.E. Stanford, "Low-Frequency Fluctuations of a CW Signal in the Ocean," J. Acoust. Soc. Am., 55, p. 968, 1974.

50. R.P. Porter and R.C. Spindel, "Low-Frequency Acoustic Fluctuations and Internal Gravity Waves in the Ocean," J. Acoust. Soc. Am., 61, p. 943, 1977.

51. F. Dyson, W. Munk, and B. Zetler, "Interpretation of Multipath Scintillations Eleuthera to Bermuda in Terms of Internal Waves and Tides," J. Acoust. Soc. Am., 59, p. 1121, 1976.

52. R.F. Dashen, S.M. Flatte, W.H. Munk, and F. Zachariasen, "Limits on Coherent Processing Due to Internal Waves," SRI Tech. Report JSR-76-14 (1977).

53. I. Dyer, "Fluctuations--An Overview," International Workshop on Low Frequency Propagation and Noise, Woodshole, MA, 14-19 Oct. 1974, Vol I (VI), p. 365, Maury Center for Ocean Science, Wash., D.C., 1977.

54. J.G. Clark, R.P. Flanagan, and N.L. Weinberg, "Multipath Acoustic Propagation with a Moving Source in a Bounded Deep Ocean Channel," J. Acoust. Soc. Am., 60, p. 1274, 1976.

55. B. Williams and F. Fisher, Private Communications.

56. M.Z. Lawrence and D.J. Ramsdale, "Comparison of Vertical Line Array Data Taken at Two Depths in the Deep Ocean," J. Acoust. Soc. Am., 77 (51), Paper GG6, 1985.

57. H. Cox, "Approximate Ray Angle Diagram," J. Acoust. Soc. Am., 61 (2), pp. 353-369, 1977.

58. E.P. Jensen and H. Cox, "Fluctuations in the Signal Response of Vertical Arrays Caused by Source Motion," J. Acoust. Soc. Am., 50 (SI), Paper 211, 1975.

59. K.M. Guthrie and C.T. Tindle, "Ray Effects in the Normal Mode Approach to Underwater Acoustics," J. Sound Vib., 47, pp. 403-413, 1976.

60. B.G. Roberts, "Horizontal-Gradient Acoustic Ray-Trace Program Trimain," NRL Report 7827, NRL, Wash., D.C., 1974.

61. H.P. Bucker, "Sound Propagation in a Channel with Lossy Boundaries," J. Acoust. Soc. Am., 48 (5), pp. 1187-1194, 1970.

62. W.M. Carey and N. Yen, "The Formation of Synthetic Aperture with Towed Hydrophones," Presented at the 107th Meeting of the Acoustical Society of America, paper GG6, 9 Mar. 1984, Norfolk, VA. Also NORDA SP80:84:13, NORDA, NSTL, MS 39529.

63. R.C. Spindel and R.P. Porter, "Long-Range, Low Frequency Acoustic Amplitude and Phase Fluctuations at Two Frequencies," J. Acoust. Soc. Am., 50 (31), pp. 712, 1975.

64. K. Kovaly, Synthetic Aperture Radar, Artech House Inc., Dedham, MA, 1978.

65. L. Cutrona, "Comparison of Sonar System Performance Achievable Using Synthetic Aperture Technique with Performance Achievable by More Conventional Means," J. Acoust. Soc. Am., 58, 336-348, 1975.

## INITIAL DISTRIBUTION LIST

| Addressee | No. of Copies |
|---|---|
| DTIC | 1 |
| DARPA (NTO C. Stuart and A. Ellinthorpe) | 2 |
| OCNR-00, -10, -11, -122, -13 (5), -20 (2) | 11 |
| ONR DET BAY ST. LOUIS | 1 |
| ONR DET BOSTON | 1 |
| ONR DET PASADENA | 1 |
| NAIR-03, -340 | 2 |
| PDW-124 | 2 |
| SPAWAR-05 | 1 |
| SEA-63 | 2 |
| NRL-5160 (2), -5120 (2), -5100 | 5 |
| NORDA-200 (W. Moseley) | 5 |
| NOSC-711 (J. Reese, H. Bucker) | 2 |
| DTNSRDC | 2 |
| NSWC | 2 |
| NUSC DET, WEST PALM BEACH, FL | 2 |
| NPS | 1 |
| APPLIED PHYSICS LAB, JOHNS HOPKINS | 2 |
| APPLIED PHYSICS LAB, U. WASH. | 2 |
| APPLIED RESEARCH LAB, PENN STATE (D. McGammon) | 2 |
| APPLIED RESEARCH LAB, U. TEXAS | 2 |
| MARINE PHYSICAL LABORATORY SCRIPPS | 2 |
| WOODS HOLE OCEANOGRAPHIC INSTITUTION | 2 |